End Plate and Side Wall Currents in Circular Cylinder Cavity Resonator

By J. P. KINZER and I. G. WILSON

Formulas are given for the calculation of the current streamlines and intensity in the walls of a circular cylindrical cavity resonator. Tables are given which permit the calculation to be carried out for many of the lower order modes.

The integration of $\int_0^x \frac{J_\ell(x)}{J'_\ell(x)}\,dx$ is discussed; the integration is carried out for $\ell = 1$, 2 and 3 and tables of the function are given.

The current distribution for a number of modes is shown by plates and figures.

Introduction

In waveguides or in cavity resonators, a knowledge of the electromagnetic field distribution is of prime importance to the designer. Representations of these fields for the lower modes in rectangular, circular and elliptical waveguide, as well as coaxial transmission line, have frequently been described.

For the most part, however, these representations have been diagrammatic or schematic, intended only to give a general physical picture of the fields. In actual designs, such as high Q cavities for use as echo boxes,[1] accurately made plates of the distributions were found necessary to handle adequately problems of excitation of the various modes and of mode suppression.

One use of the charts is to determine where an exciting loop or orifice should be located and how the field should be oriented for maximum coupling to a particular mode. Optimum locations for both launchers and absorbers can be found. Naturally, when attention is concentrated on a single mode these will be located at the maximum current density points. If, however, two or more modes can coexist, and only one is desired, compromise locations can sometimes be found which minimize the unwanted phenomena.

Also, in a cylindrical cavity resonator of high Q with diameter large compared with the operating wavelength, there are many high order modes of oscillation whose resonances fall within the design frequency band. Some of these are undesired and one of the objectives of a practical design is to reduce their responses to a tolerable amount. This process is termed

[1] "High Q Resonant Cavities for Microwave Testing," Wilson, Schramm, Kinzer, *B.S.T.J.*, July 1946.

"suppression of the extraneous modes". In this process, an exact knowledge of the distribution of the currents in the cavity walls has been found highly useful.

For example, it has been found experimentally that annular cuts in the end plates of the cylinder give a considerable amount of suppression to many types of extraneous modes with very little effect on the performance of the desired *TE* 01n mode. These cuts are narrow slits concentric with the axis of the cylinder and going all the way through the metallic end plates into a dielectric beyond.[2] The physical explanation is that an annular slit cuts through the lines of current flow of the extraneous modes, and thereby interrupts the radial component of current and introduces an impedance which damps, or suppresses, the mode. For the *TE* 01n mode, the slits

	TE Modes	*TM* Modes
End Plates	$H_\rho = \frac{k_3}{k_1} J'_\ell(k_1\rho) \cos \ell\theta$ $H_\theta = -\ell \frac{k_3}{k_1} \frac{J_\ell(k_1\rho)}{k_1\rho} \sin \ell\theta$	$H_\rho = \ell \frac{J_\ell(k_1\rho)}{k_1\rho} \sin \ell\theta$ $H_\theta = J'_\ell(k_1\rho) \cos \ell\theta$
Side Walls	$H_\theta = \left[-\ell \frac{k_3}{k_1} \frac{J_\ell(k_1 D/2)}{k_1 D/2}\right] [\sin \ell\theta \cos k_3 z]$ $H_z = J_\ell(k_1 D/2) \cos \ell\theta \sin k_3 z$	$H_\theta = J'_\ell(k_1 D/2) \cos \ell\theta \cos k_3 z$ $H_z = 0$

$$k = \frac{2\pi}{\lambda} = k_1^2 + k_3^2$$

$$k_1 = \frac{2r}{D} \qquad k_3 = \frac{n\pi}{L}$$

r = m^{th} root of $J_\ell(x) = 0$ for *TM* Modes.
= m^{th} root of $J'_\ell(x) = 0$ for *TE* Modes.

D = cavity diameter

L = cavity length

Fig. 1—Components of H vector at walls of circular cylinder cavity resonator.

are parallel to the current streamlines and there is no such interruption; presumably there is a slight increase in current density alongside the slit,

[2] Similar cuts through the side wall of the cylinder in planes perpendicular to the cylinder axis are also beneficial, but are more troublesome mechanically.

as the current formerly on the surface of the removed metal crowds over onto the adjacent metal, but this is a second-order effect.

To determine the best location of such cuts, therefore, it is necessary to know the vector distributions of the wall currents for the various modes. This current vector, I, is proportional to and perpendicular to the magnetic vector, H, of the field at the surface. Expressions for the components of the H-vector at the surfaces of the end plates and side walls are given in Fig. 1.

END PLATE: *Contour Lines*

At the end plates, the magnitude of the H-vector at any point is given by:

$$H^2 = H_\rho^2 + H_\theta^2. \tag{1}$$

Now substitute values of H_ρ and H_θ from Fig. 1 into (1); drop any constant factors common to H_ρ and H_θ as these can be swallowed in a final proportionality constant; introduce the new variable x:

$$x = k_1\rho = r\frac{\rho}{R}. \tag{2}$$

where $R = D/2$ = cavity radius. Thus is obtained:

$$H^2 = [J'_\ell(x)\cos \ell\theta]^2 + \left[\frac{\ell}{x} J_\ell(x) \sin \ell\theta\right]^2. \tag{3}$$

Now J_ℓ and J'_ℓ, are expressed in terms of $J_{\ell-1}$ and $J_{\ell+1}$ and a further reduction leads to:

$$H^2 = (J_{\ell-}\cos \ell\theta)^2 + (J_{\ell+}\sin \ell\theta)^2 \tag{4}$$

where

$$J_{\ell-} = J_{\ell-1}(x) - J_{\ell+1}(x) \tag{5}$$

and

$$J_{\ell+} = J_{\ell-1}(x) + J_{\ell+1}(x) \tag{6}$$

The formulas (4) to (6) apply to both TE and TM modes. The values obtained depend on r, which is different for each mode.

When $\theta = 0$, I is proportional to $J_{\ell-}$ and when $\theta = \pi/2\ell$, I is proportional to $J_{\ell+}$. Relative values of I are thus easily calculated for these cases, once tables of J_ℓ are available. Such tables have been prepared and are attached. For TE modes, when $\theta = 0$, $H_\theta = 0$, and the currents are all in the θ direction. For TM modes, when $\theta = 0$, $H_\rho = 0$, and the currents are all in the ρ-direction. When $\theta = \pi/2\ell$, the converse holds.

Figures 3 to 18 are a set of curves showing the relative magnitude of H (or I) for several of the lower order TE and TM modes. The abscissae

are relative radius, i.e., ρ/R; the ordinates are relative magnitude referred to the maximum value. The drawings also give $r = \pi D/\lambda_c$ for each mode, where λ_c is the cutoff wavelength in a circular guide of diameter D. Values for any point of the surface of the end plate can be calculated by using these curves in conjunction with equation (4).

In general, for each mode there are certain radii at which the current flow is entirely radial, ($I_\theta = 0$). At these radii, which correspond to zeros of $J_\ell(x)$ or $J'_\ell(x)$, the annular cuts mentioned in the introduction are quite effective. However, the maxima of I_ρ do not coincide with the zeros of I_θ; and a more sophisticated treatment gives the best radius as that which maximizes ρI_ρ^2. Values of the relative radius for this last condition are given in Table IV.

Contour lines of equal relative current intensity are obtained by setting H^2 constant in (4), which then expresses a relation between x and θ. The easiest and quickest way to solve (4) is graphically, by plotting H vs. x for different values of θ.

END PLATE: *Current Streamlines*

It is easy to show that the equations of the current streamlines are given by the solutions of the differential equation

$$\frac{d\rho}{d\theta} = -\rho \frac{H_\theta}{H_\rho}. \tag{7}$$

In the case of the TE modes, (7) is easily solved by separation of the variables, leading to the final result:

$$J_\ell(x) \cos \ell\theta = C \tag{8}$$

in which C is a parameter whose value depends on the streamline under consideration. In the TE modes, the E-lines in the interior of the cavity also satisfy (8), hence a plot of the current streamlines in the end plate serves also as a plot of the E lines.

In the case of the TM modes, (7) is not so easily solved. Separation of the variables leads to:

$$-\log \sin \ell\theta = \int \frac{\ell^2 J_\ell(x)}{x^2 J'_\ell(x)}\, dx. \tag{9}$$

The right-hand side of (9) can be reduced somewhat, yielding

$$-\log \sin \ell\theta = \log [xJ'_\ell(x)] + \int \frac{J_\ell(x)}{J'_\ell(x)}\, dx \tag{10}$$

but no further reduction is possible. The remaining integral represents a new function which must be tabulated. Its evaluation is discussed at

length in the Appendix, where it is denoted by $F_\ell(x)$. Table II of the Appendix gives its values (for $\ell = 1, 2$ and 3) and also those of $G_\ell(x)$ where

$$F_\ell(x) = -\log G_\ell(x) \tag{11}$$

Thus (10) becomes

$$-\log \sin \ell\theta = \log [x J'_\ell(x)/G_\ell(x)] + C' \tag{12}$$

and the final equation for the current streamlines is

$$[xJ'_\ell(x)/G_\ell(x)] \sin \ell\theta = C \tag{13}$$

where C is a parameter as before.

It is not difficult to show that $G_\ell(x)/J'_\ell(x)$ has zeros at the zeros of $J'_\ell(x)$. For these values of x, $\sin \ell\theta = 0$ whatever the value of C, and all streamlines converge on (or diverge from) $2\ell m$ points on the end plate.

The flow lines of (13) are orthogonal to the family (8) and could readily be drawn in this manner. However, better accuracy is obtained by plotting (13).

END PLATE: *Distributions*

The 32 attached plates show the distribution of current in the end plates of a circular cylinder cavity resonator for a number of modes.

In the first set of 21, the scaling is such that the diameters of the figures are proportional to those of circular waveguides which would have the same cutoff frequency. This group is of particular interest to the waveguide engineer.

In a second group of 11, the scaling is such as to make the outside diameters of the cylinders uniform. This group is of particular interest to a cavity designer.

This distribution is a vector function of position; that is, at each point in the end plate the surface current has a different direction of flow and a different magnitude or intensity. The variation in current intensity is represented by ten degrees of background shading. The lightest indicates regions of least current intensity and the darkest greatest intensity. The direction of current flow is shown by streamlines. Streamlines are lines such that a tangent at any point indicates the direction of current flow at that point.

The modes represented are the

TE 01, 02, 03	*TM* 01, 02, 03
TE 11, 12, 13	*TM* 11, 12, 13
TE 21, 22, 23	*TM* 21, 22
TE 31, 32	*TM* 31, 32

in the nomenclature which has become virtually standard. In this system, *TE* denotes transverse electric modes, or modes whose electric lines lie in planes perpendicular to the cylinder axis; *TM* denotes transverse magnetic modes, or modes whose magnetic lines lie in transverse planes. The first numerical index refers to the number of nodal diameters, or to the order of the Bessel function associated with the mode. The second numerical index refers to the number of nodal circles (counting the resonator boundary as one such) or to the ordinal number of a root of the Bessel function associated with the mode. On the end plates, the distribution does not depend upon the third index (number of half wavelengths along the axis of the cylinder) used in the identification of resonant modes in a cylinder. This considerably simplifies the problem of presentation. The orientation of the field inside the cavity and hence the currents in the end plate depend on other things; thus the orientation of the figures is to be considered arbitrary.

The plates also apply to the corresponding modes of propagation in a circular waveguide as follows: The background shading represents the instantaneous relative distribution of energy across a cross section of guide. For *TE* modes, the current streamlines depict the *E* lines; for the *TM* modes, they depict the projection of the *E* lines on a plane perpendicular to the cylinder axis.

SIDE WALL:

The current distribution in the side walls is easily obtained from the field equations of Fig. 1. For *TM* modes, the currents are entirely longitudinal; their magnitudes vary as $\cos \ell\theta \cos n\pi z/L$. This distribution is so simple as not to require plotting.

For *TE* modes, the situation is more complicated, since both H_z and H_θ exist along the side wall. The current streamlines are given by the solutions of the differential equation

$$\frac{dz}{d\theta} = -\frac{DH_\theta}{2H_z}. \tag{14}$$

By separation of the variables, the solution is found to be

$$\log (C \cos \ell\theta) = \left[\frac{k_1}{k_3}\right]^2 \log \cos k_3 z. \tag{15}$$

Contour lines of constant magnitude of the current are given by

$$\left(\frac{2k_3 \ell}{k_1^2 D} \sin \ell\theta \cos k_3 z\right)^2 + (\cos \ell\theta \sin k_3 z)^2 = K^2. \tag{16}$$

In the above, C and K are parameters, different values of which correspond to different streamlines or contour lines, respectively.

Since both streamlines and contours are periodic in z and θ, it is not essential to represent more than is covered in a rectangular piece of the side wall corresponding to quarter periods in z and θ. These are covered in a length $\frac{L}{2n}$ along the cavity and in a distance $\frac{\pi D}{4\ell}$ around the cavity. If such a piece of the surface be rolled out onto a plane it forms a rectangle of proportions $\frac{\pi nD}{2\ell L}$.

The difficulty in depicting the side wall currents of TE modes, as compared with the end plate currents, is now apparent. For the end plate, the "proportions" are fixed as being a circle. Furthermore, for a given ℓ, as m increases the effect is merely to add on additional rings to the previous streamline and contour plots. Here, however, the proportions of the rectangle are variable, in the first place. And for a given rectangle the streamlines and contours both change as ℓ and m are varied. Another way of expressing the same idea is that for end plates the current distribution does not depend upon the mode index n, and varies only in an additive way with the index m, whereas for the side walls the distribution depends in nearly equal strength on ℓ, m and n.

Some simplification of the situation is accomplished by introducing two new parameters, the "shape" and the "mode" parameters, defined by:

$$S = \frac{\pi nD}{2\ell L} \qquad M = \frac{\ell}{r} \tag{17}$$

and two new variables

$$Z = k_3 z \qquad \phi = \ell\theta. \tag{18}$$

Substitution of the above, and also the expressions for k_1 and k_3 (see Fig. 1) into (15) and (16) yields

$$\cos Z = C(\cos\phi)^{S^2M^2} \quad \text{(streamlines)} \tag{19}$$

$$\cos Z = \left[\frac{K^2 - \cos^2\phi}{(S^2M^4\sin^2\phi - \cos^2\phi)}\right]^{1/2} \quad \text{(contours)}. \tag{20}$$

For given proportions S, one can calculate the streamlines and contours for various values of M. Thus a "square array" of side wall currents can be prepared, such as shown on Fig. 2.

The mode parameter, M, in the physical case takes on discrete values which depend on the mode. Some of its values are given in the following table. They all lie between 0 and 1 and there are an infinite number of them.

VALUE OF $M = \ell/r$ FOR TE MODES

ℓ	1	2	3	4	5	6	10	15	20
$m = 1$	.5432	.6549	.7141	.7522	.7793	.8000	.8495	.8813	.9001
2	.1875	.2982	.3743	.4309	.4753	.5113	.6080	.6774	
3	.1172	.2006	.2644	.3154	.3575	.3930	.4945	.5730	
4	.0854	.1519	.2057	.2506	.2888	.3219	.4209		

For any given mode in any given cavity, the values of S and M can be calculated from (17). In general, these values will not coincide with those which have been plotted, but by the same token, they will lie among a group of four combinations which have been plotted. Since the changes in distribution are smooth, mental two-way interpolation will present no difficulty.

ACKNOWLEDGMENT

The final plates depicting the current distributions are the result of the efforts of many individuals in plotting, spray tinting of the background, inking of the streamlines on celluloid overlay, and photographing. Special mention must be made, however, of the contribution of Miss Florence C. Larkey, who carried out all the lengthy calculations of the tables hereto attached and of the necessary data for the plotting.

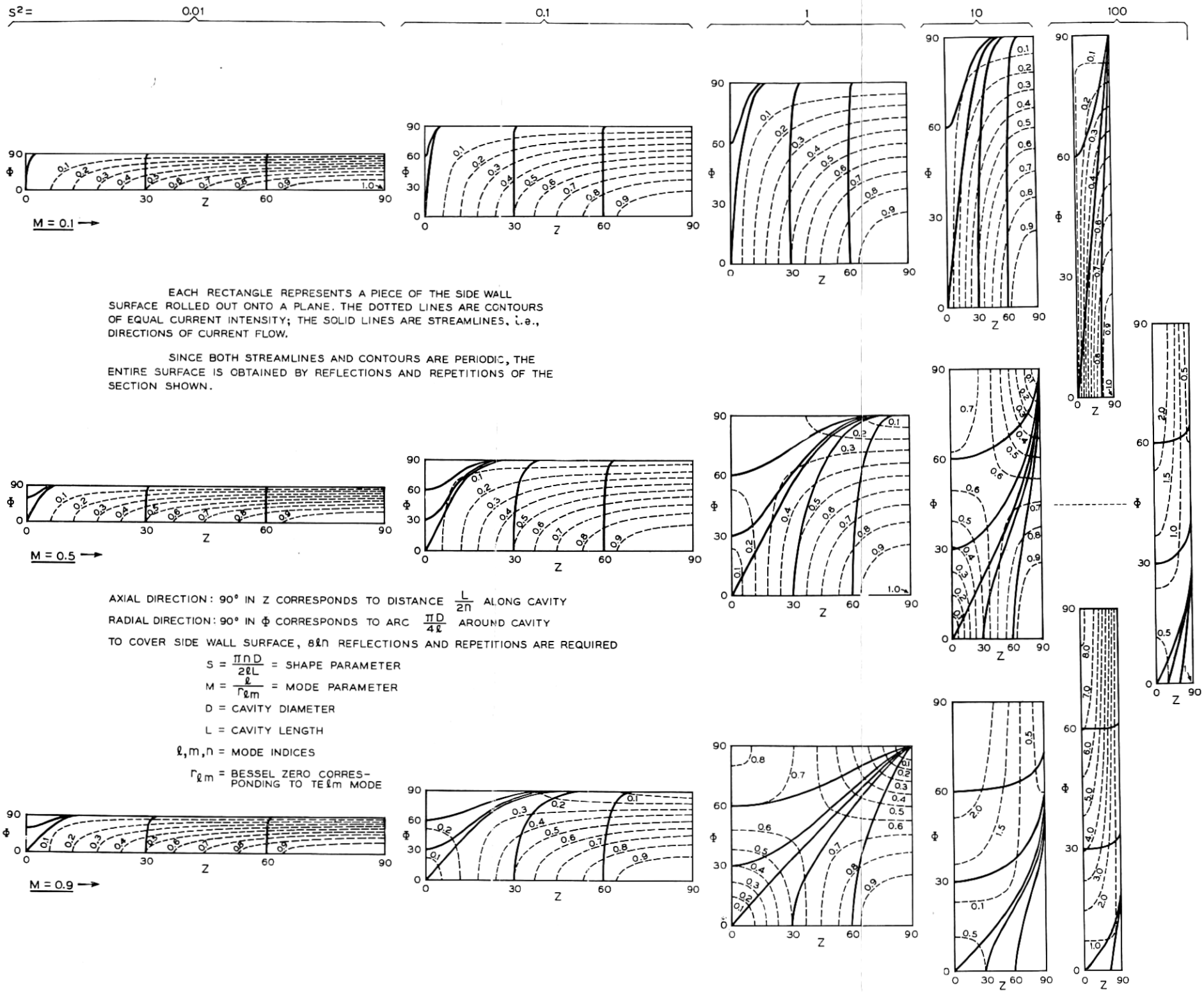

EACH RECTANGLE REPRESENTS A PIECE OF THE SIDE WALL SURFACE ROLLED OUT ONTO A PLANE. THE DOTTED LINES ARE CONTOURS OF EQUAL CURRENT INTENSITY; THE SOLID LINES ARE STREAMLINES, i.e., DIRECTIONS OF CURRENT FLOW.

SINCE BOTH STREAMLINES AND CONTOURS ARE PERIODIC, THE ENTIRE SURFACE IS OBTAINED BY REFLECTIONS AND REPETITIONS OF THE SECTION SHOWN.

AXIAL DIRECTION: 90° IN Z CORRESPONDS TO DISTANCE $\frac{L}{2n}$ ALONG CAVITY

RADIAL DIRECTION: 90° IN Φ CORRESPONDS TO ARC $\frac{\pi D}{4\ell}$ AROUND CAVITY

TO COVER SIDE WALL SURFACE, $8\ell n$ REFLECTIONS AND REPETITIONS ARE REQUIRED

$S = \frac{\pi n D}{2\ell L}$ = SHAPE PARAMETER

$M = \frac{\ell}{r_{\ell m}}$ = MODE PARAMETER

D = CAVITY DIAMETER

L = CAVITY LENGTH

ℓ, m, n = MODE INDICES

$r_{\ell m}$ = BESSEL ZERO CORRESPONDING TO TE ℓm MODE

Fig. 2—Side wall currents in circular cylinder cavity resonator for TE modes ($l > 0$).

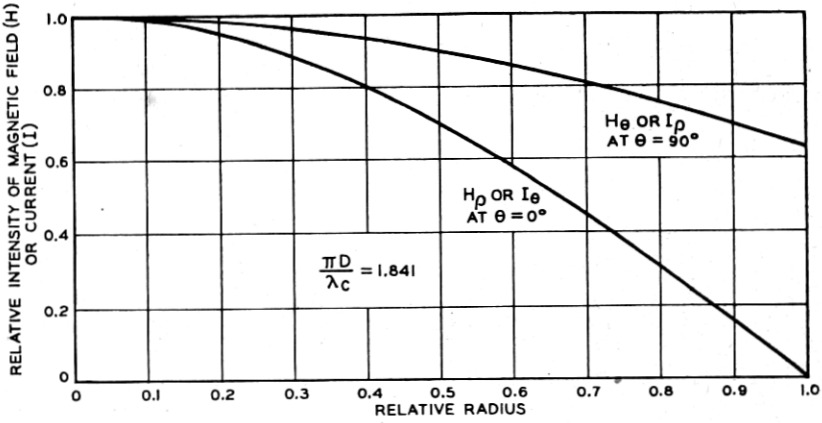

Fig. 3—End plate currents in TE 11 mode.

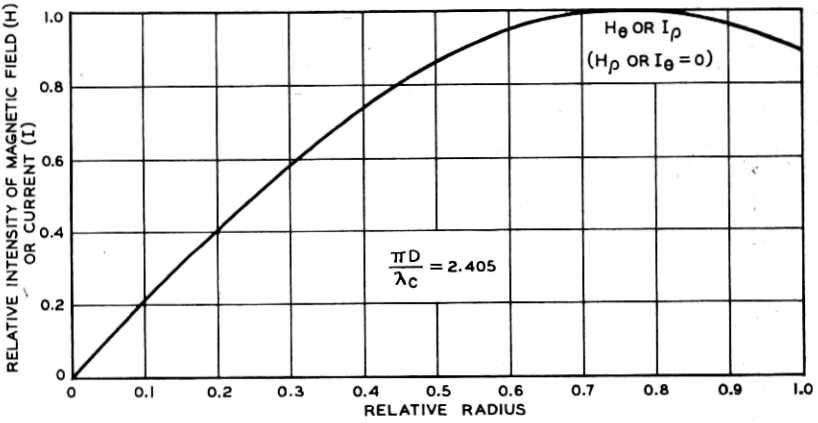

Fig. 4—End plate currents in TM 01 mode.

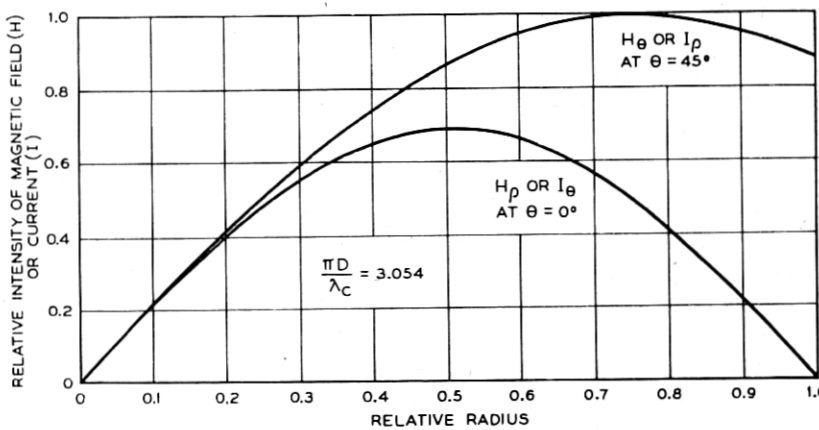

Fig. 5—End plate currents in TE 21 mode.

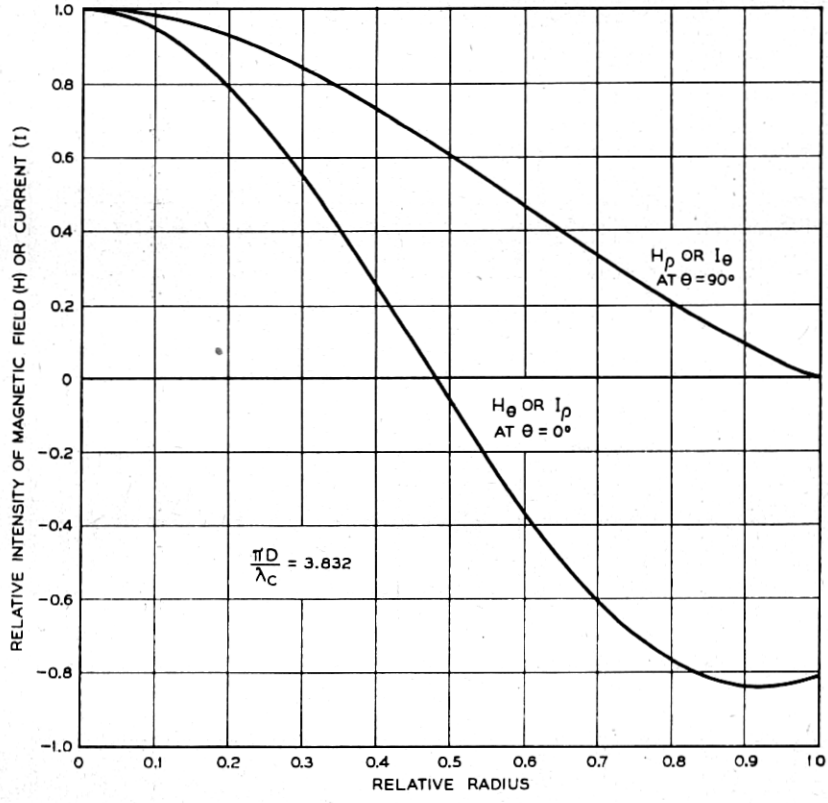

Fig. 6—End plate currents in TM 11 mode.

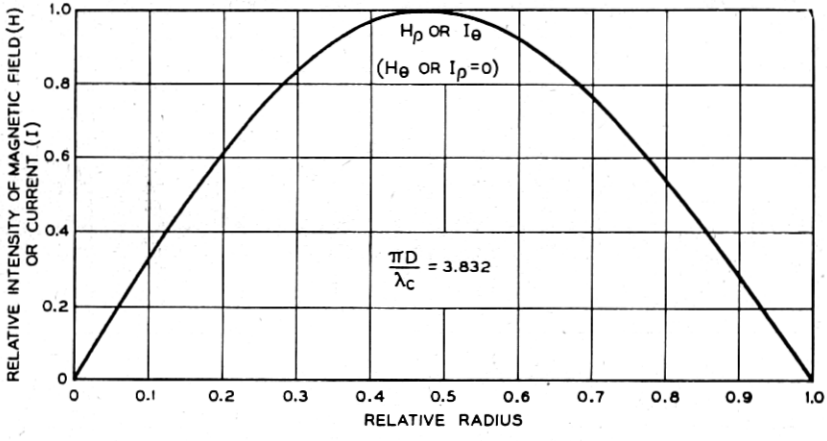

Fig. 7—End plate currents in TE 01 mode.

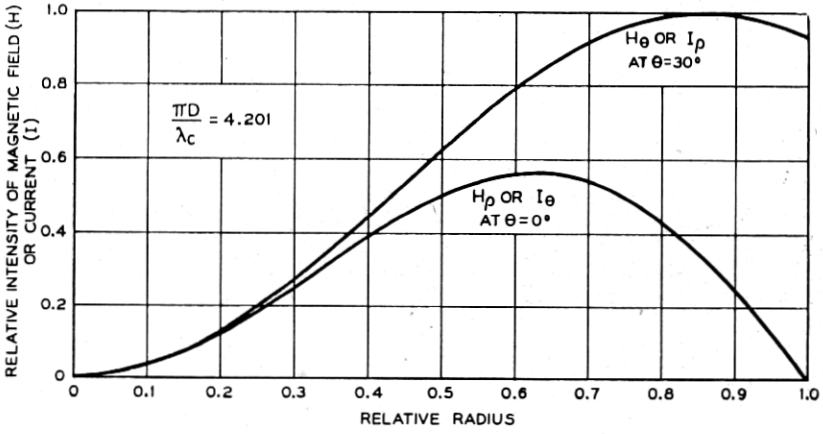

Fig. 8—End plate currents in TE 31 mode.

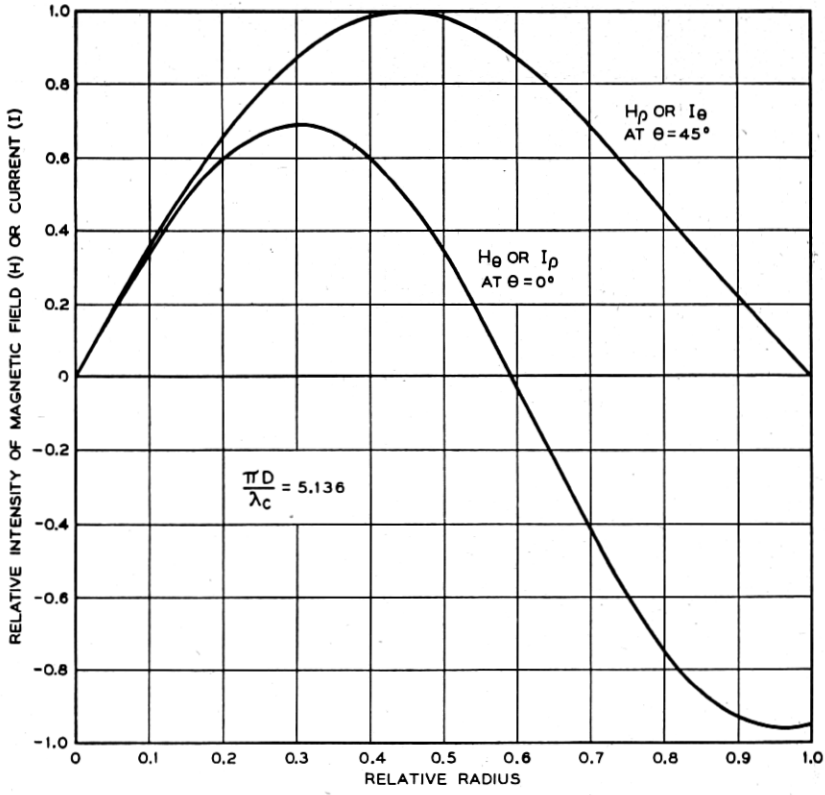

Fig. 9—End plate currents in TM 21 mode.

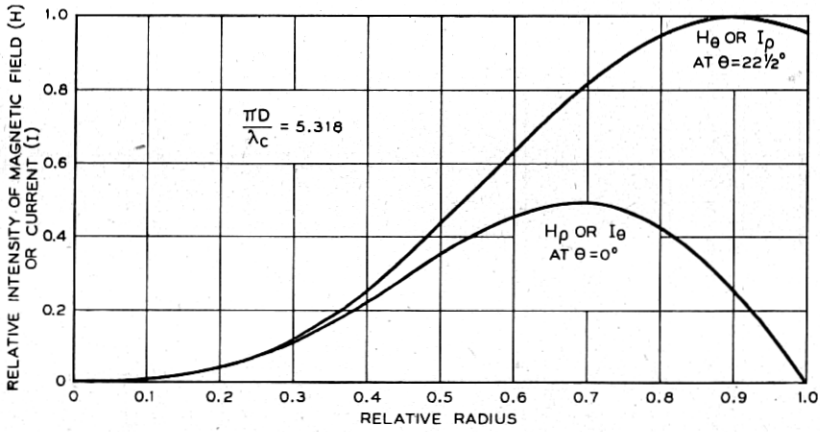

Fig. 10—End plate currents in TE 41 mode.

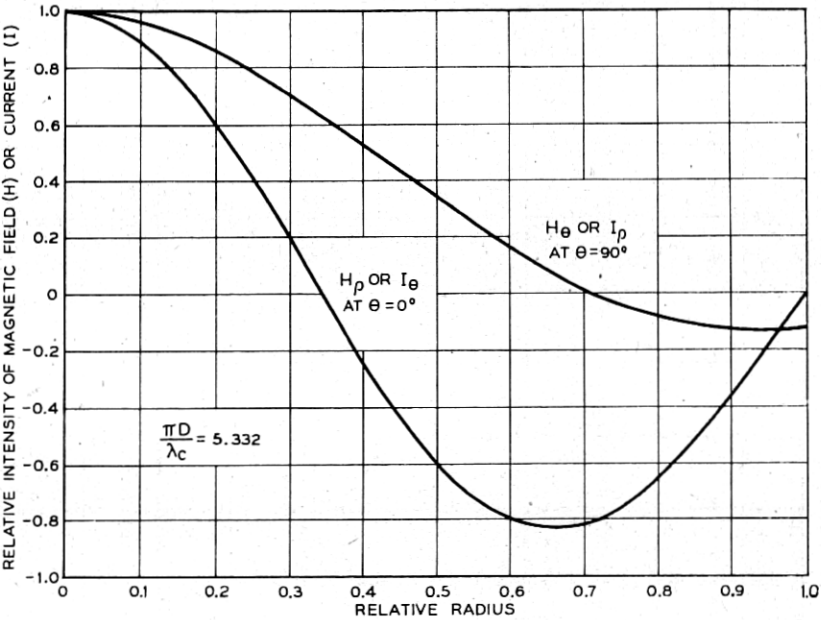

Fig. 11—End plate currents in TE 12 mode.

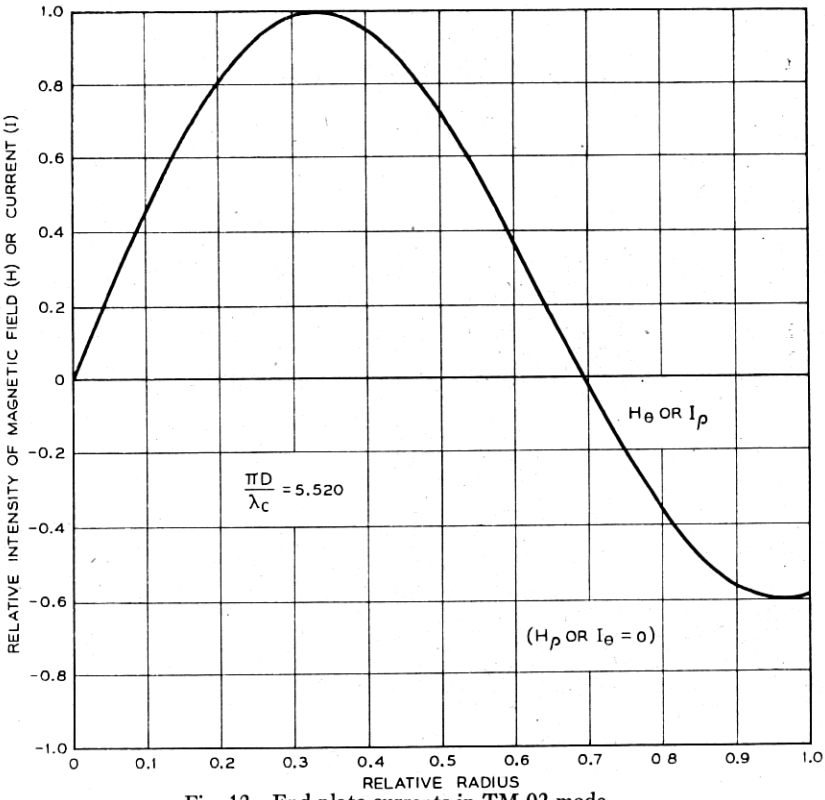

Fig. 12—End plate currents in TM 02 mode.

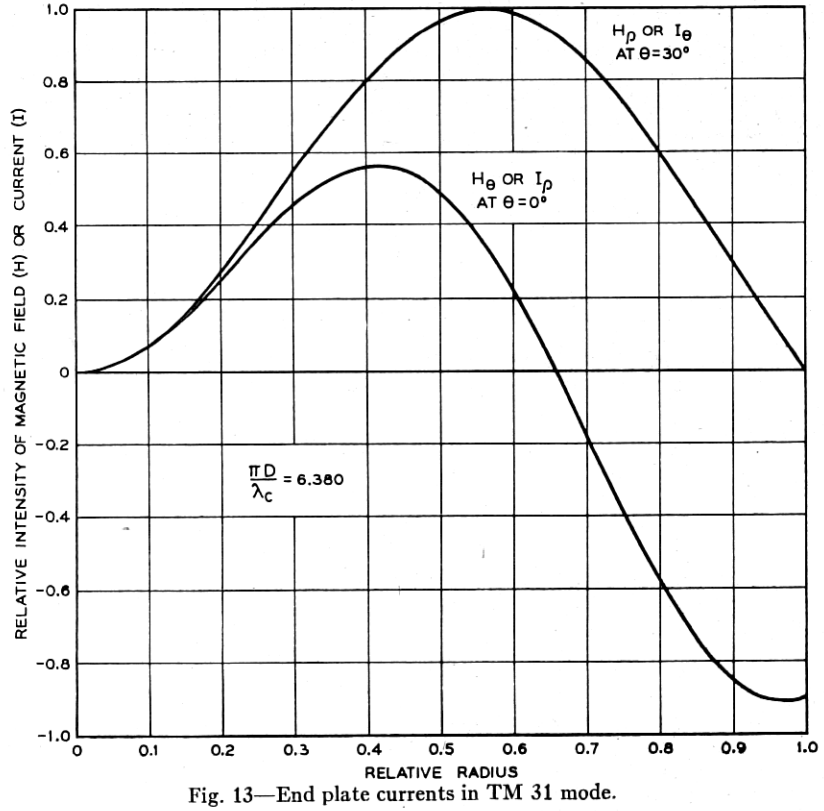

Fig. 13—End plate currents in TM 31 mode.

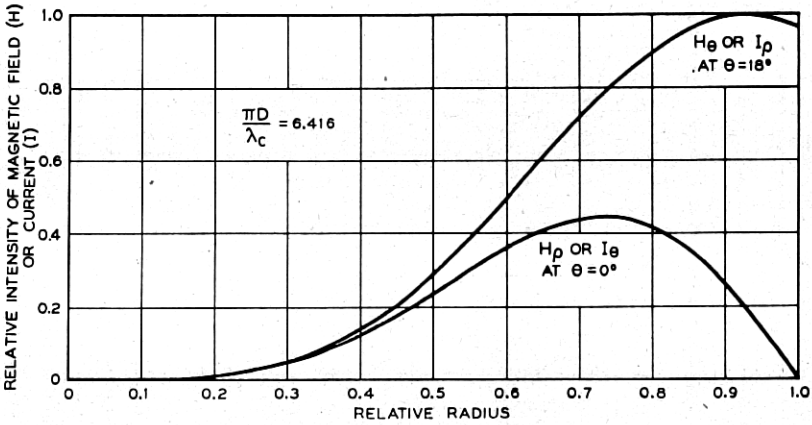

Fig. 14—End plate currents in TE 51 mode.

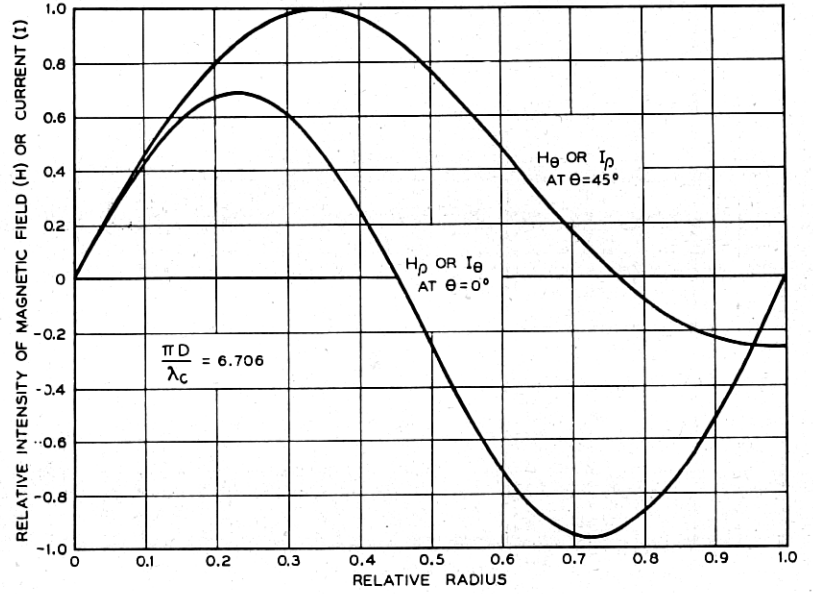

Fig. 15—End plate currents in TE 22 mode.

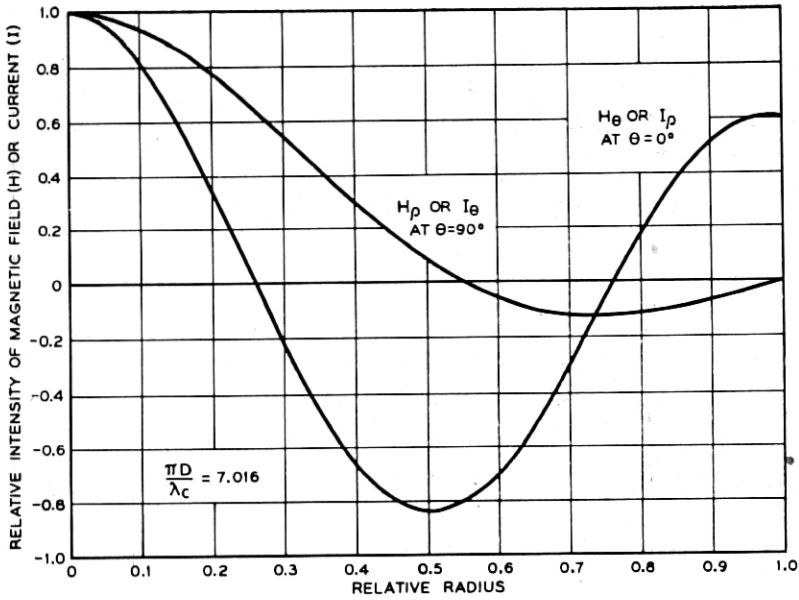

Fig. 16—End plate currents in TM 12 mode.

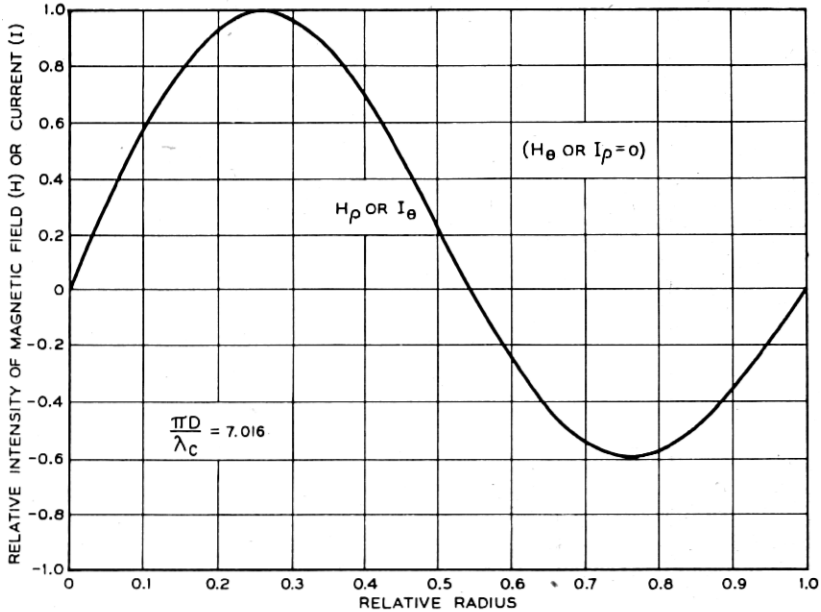

Fig. 17—End plate currents in TE 02 mode.

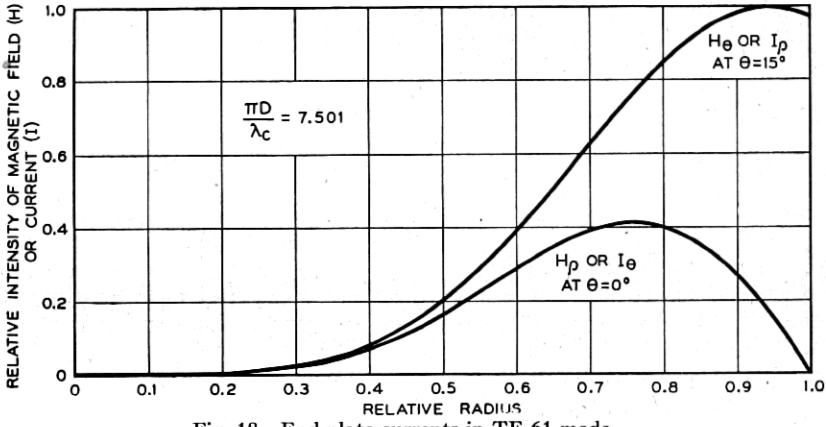

Fig. 18—End plate currents in TE 61 mode.

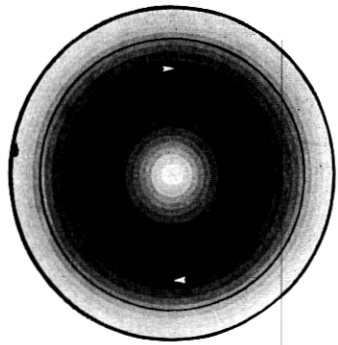

Fig. 19—TE 01 mode.

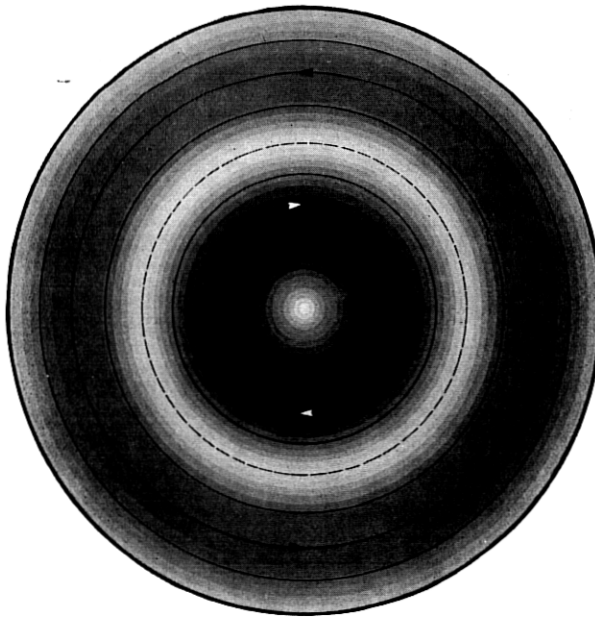

Fig. 20—TE 02 mode.

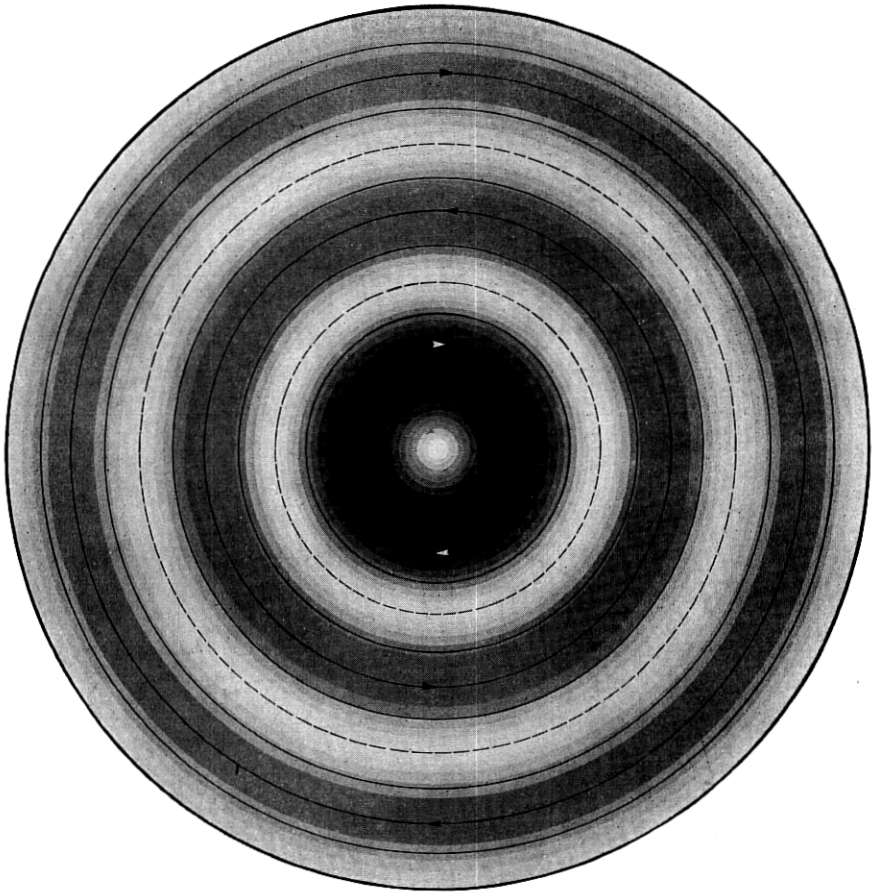

Fig. 21—TE 03 mode.

Fig. 22—TE 11 mode.

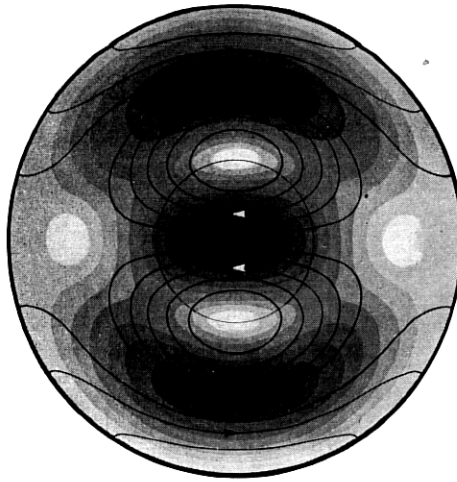

Fig. 23—TE 12 mode.

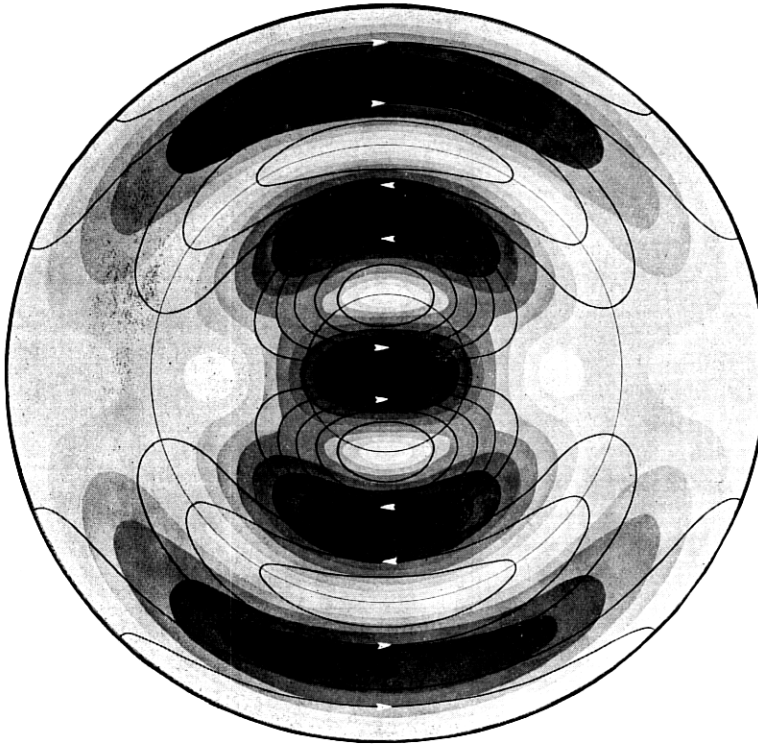

Fig. 24—TE 13 mode.

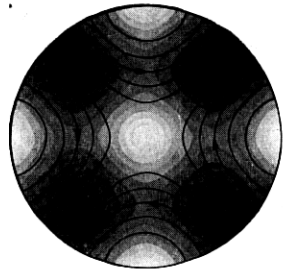

Fig. 25—TE 21 mode.

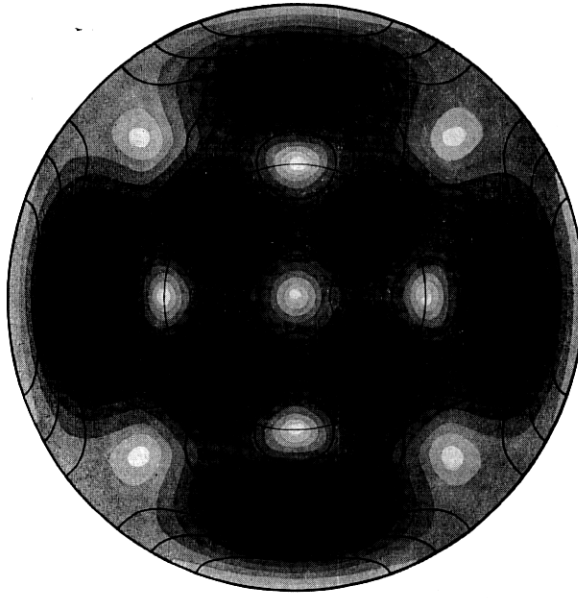

Fig. 26—TE 22 mode.

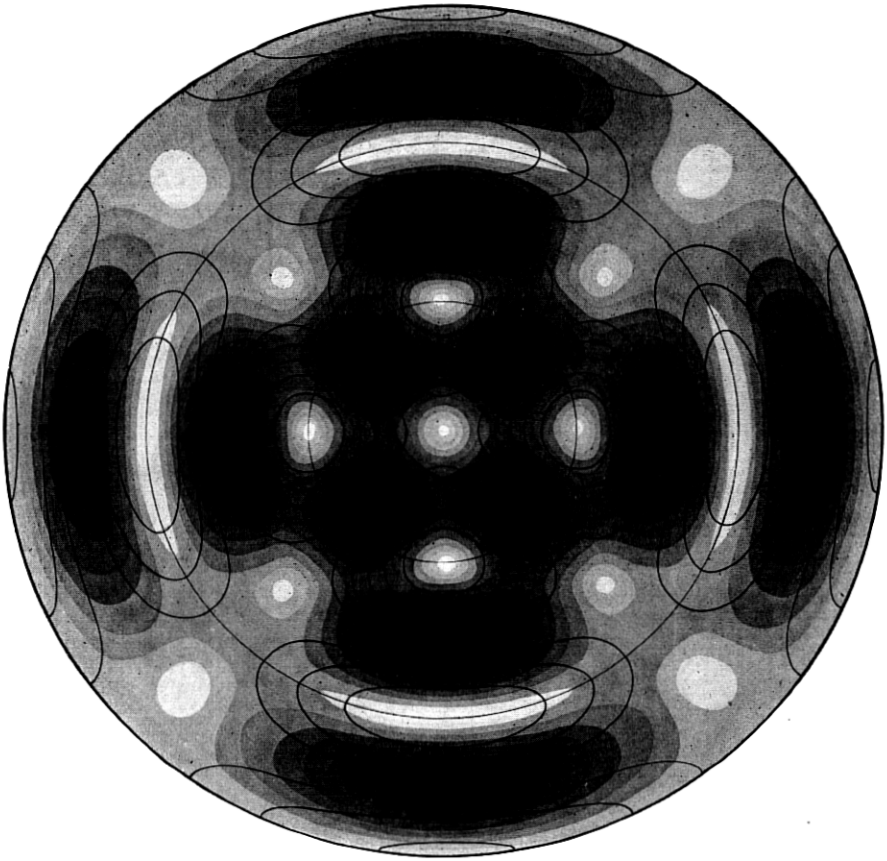

Fig. 27—TE 23 mode.

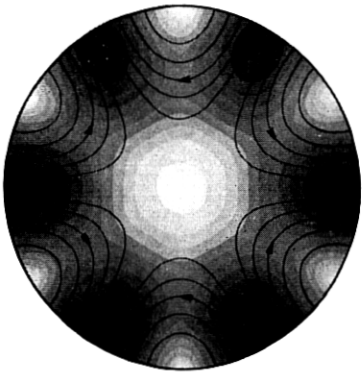

Fig. 28—TE 31 mode.

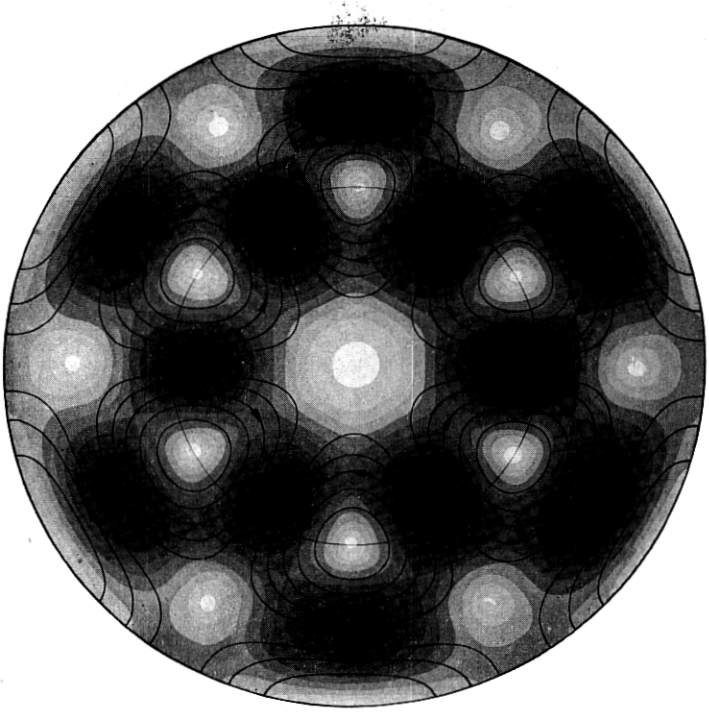

Fig. 29—TE 32 mode.

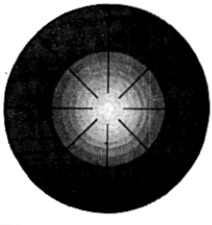

Fig. 30—TM 01 mode.

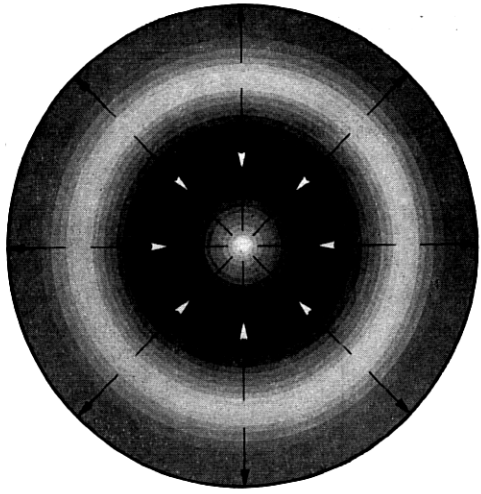

Fig. 31—TM 02 mode.

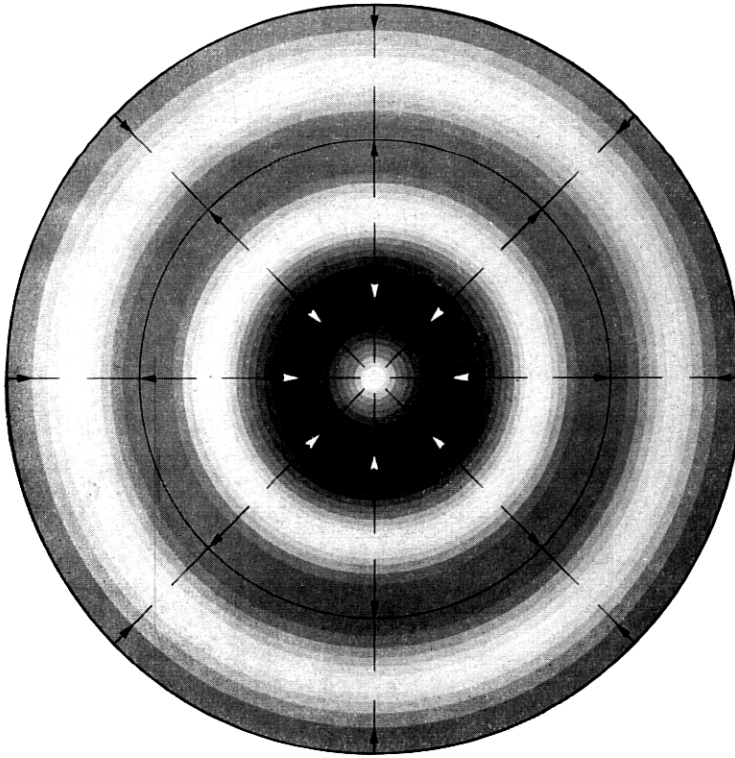

Fig. 32—TM 03 mode.

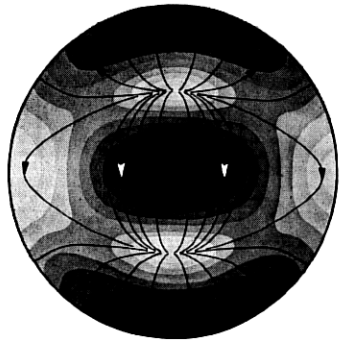

Fig. 33—TM 11 mode.

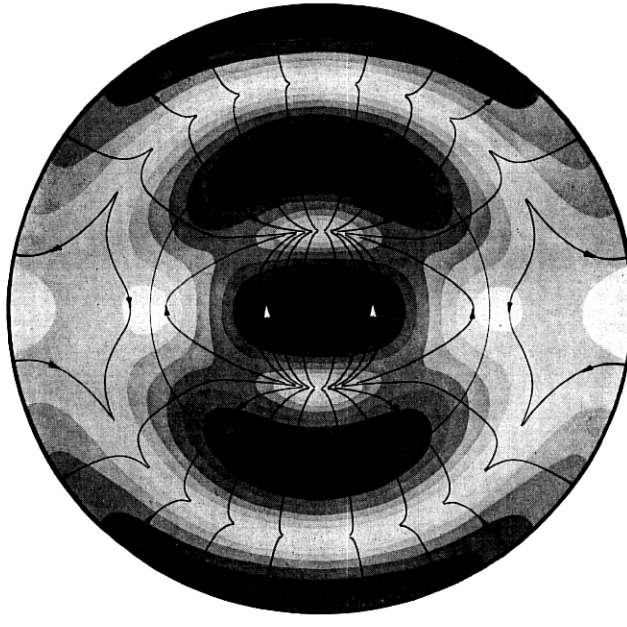

Fig. 34—TM 12 mode.

Fig. 35—TM 13 mode.

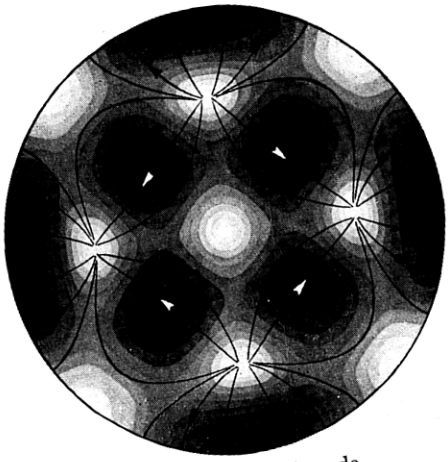

Fig. 36—TM 21 mode.

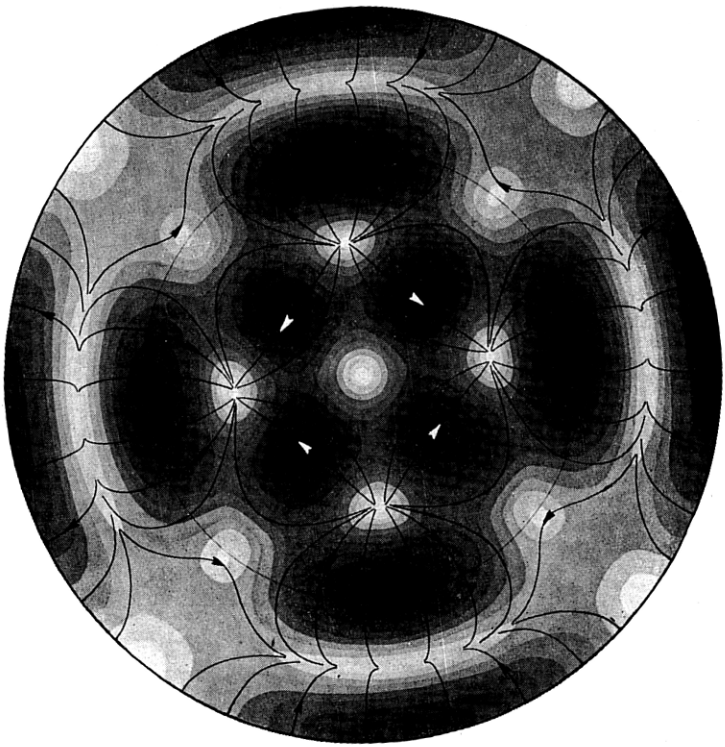

Fig. 37—TM 22 mode.

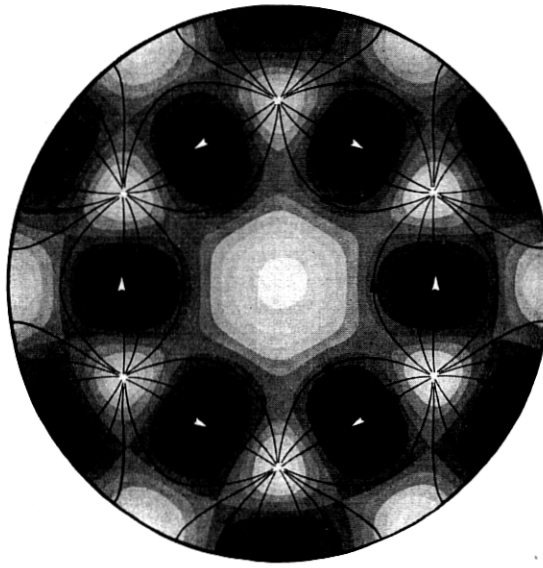

Fig. 38—TM 31 mode.

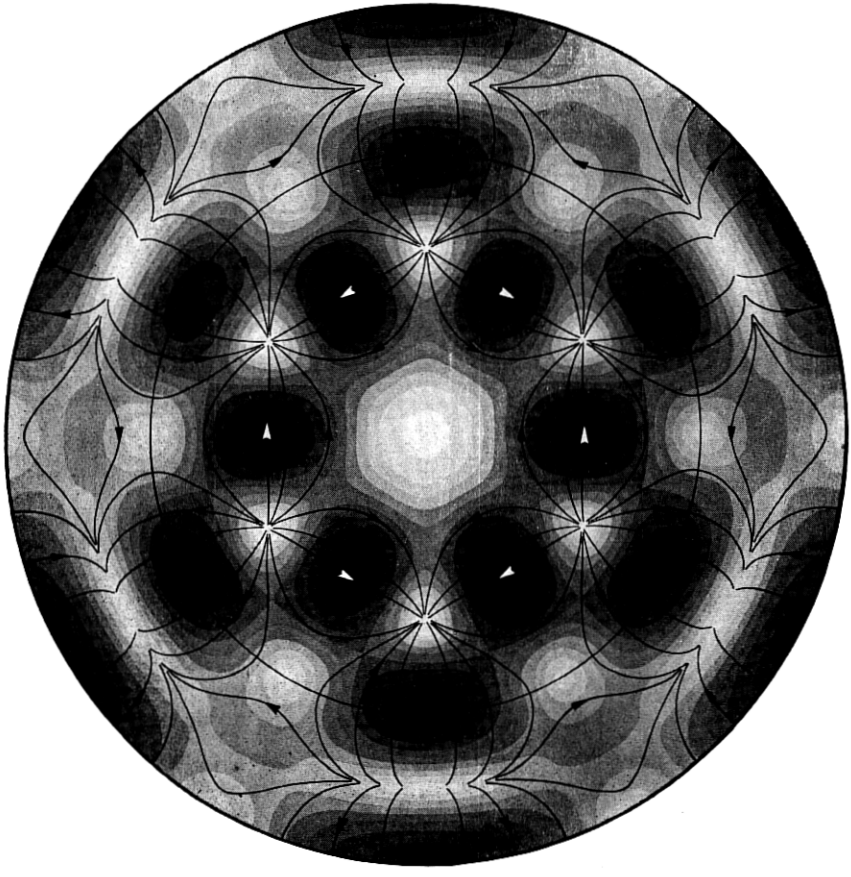

Fig. 39—TM 32 mode.

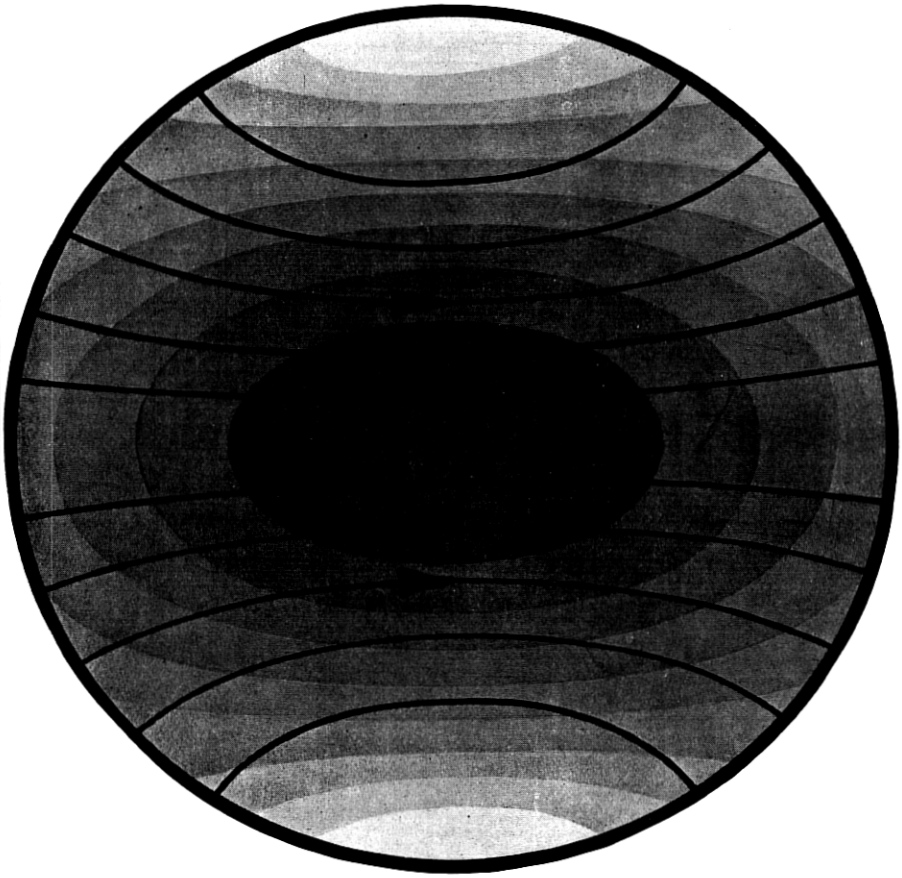

Fig. 40—TE 11 mode.

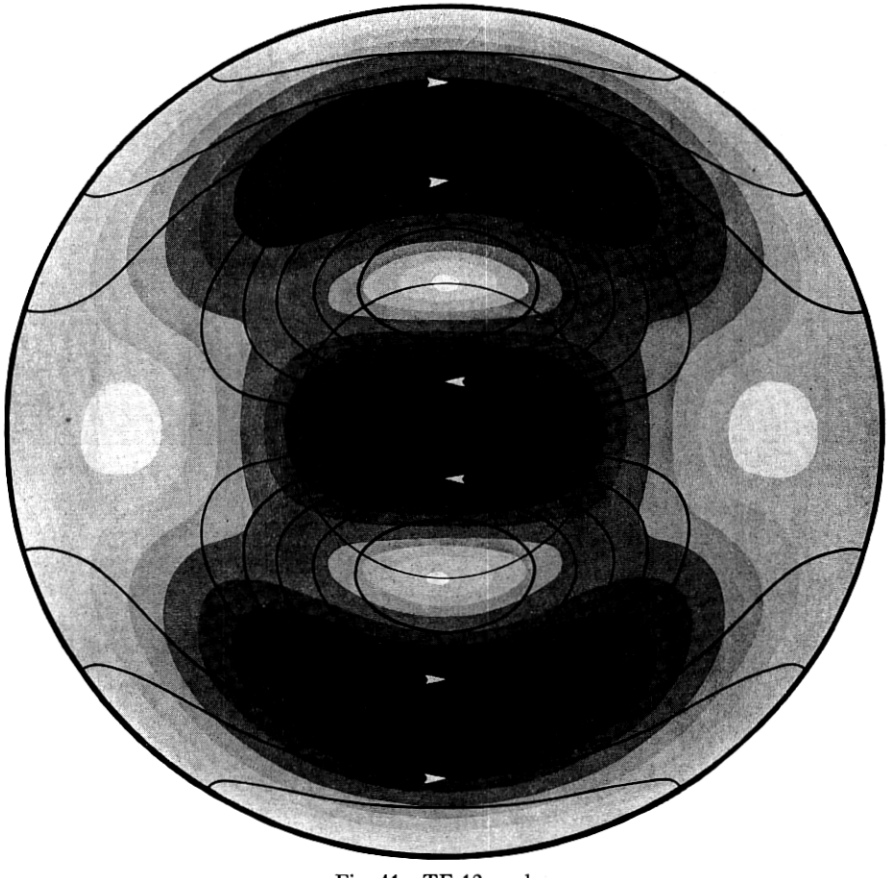

Fig. 41—TE 12 mode.

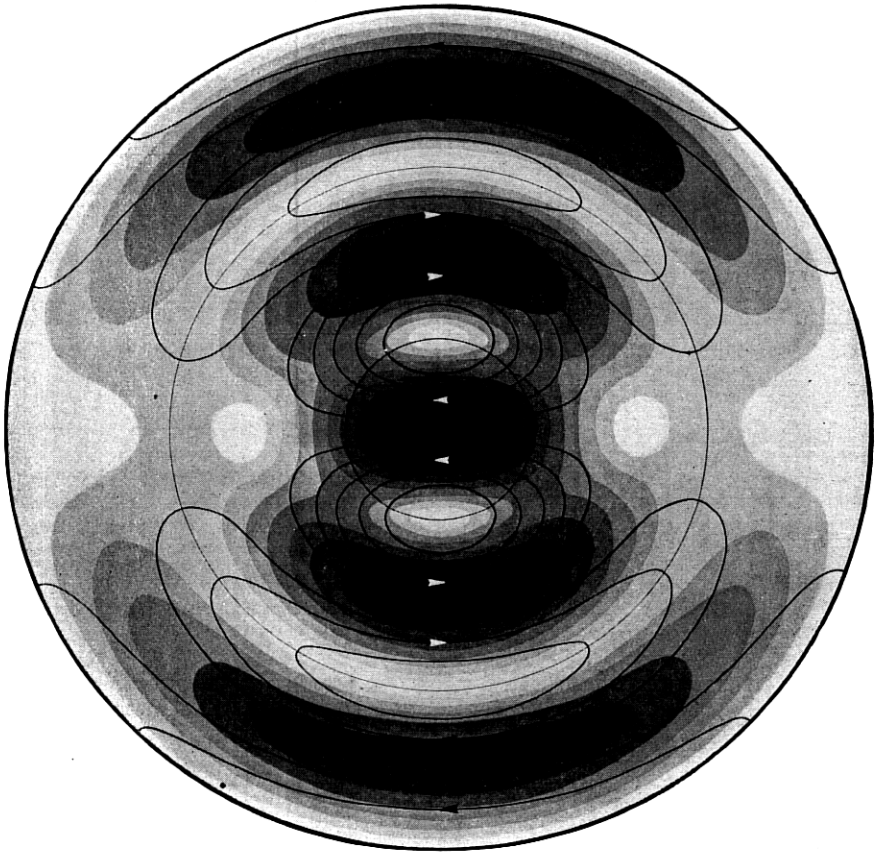

Fig. 42—TE 13 mode.

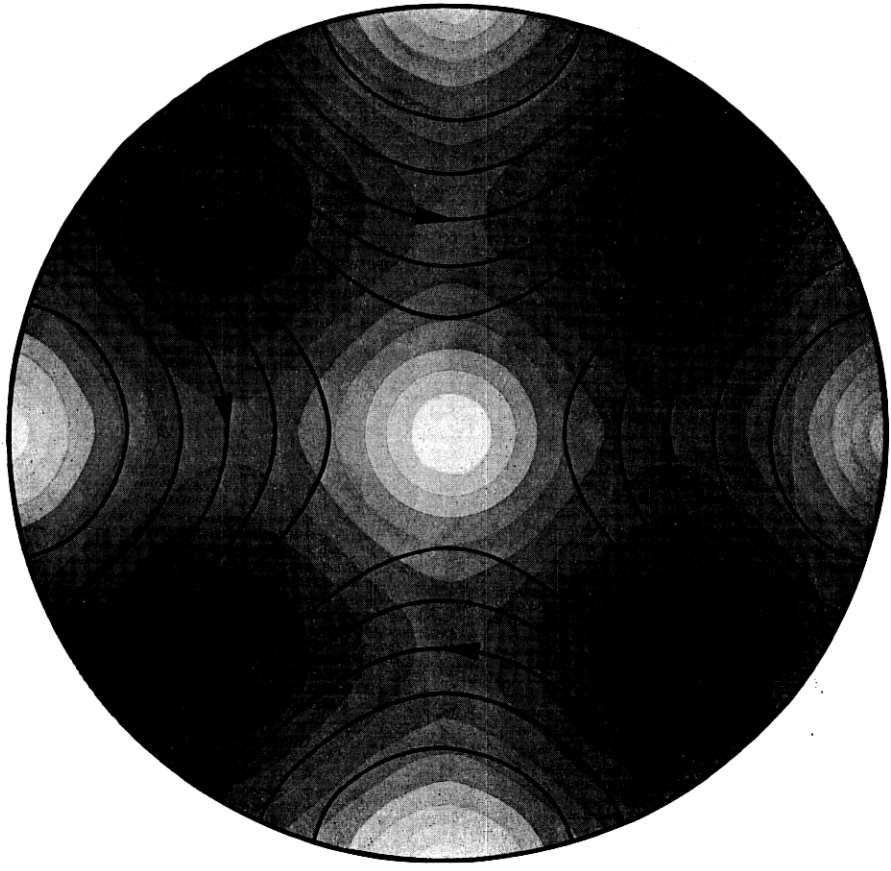

Fig. 43—TE 21 mode.

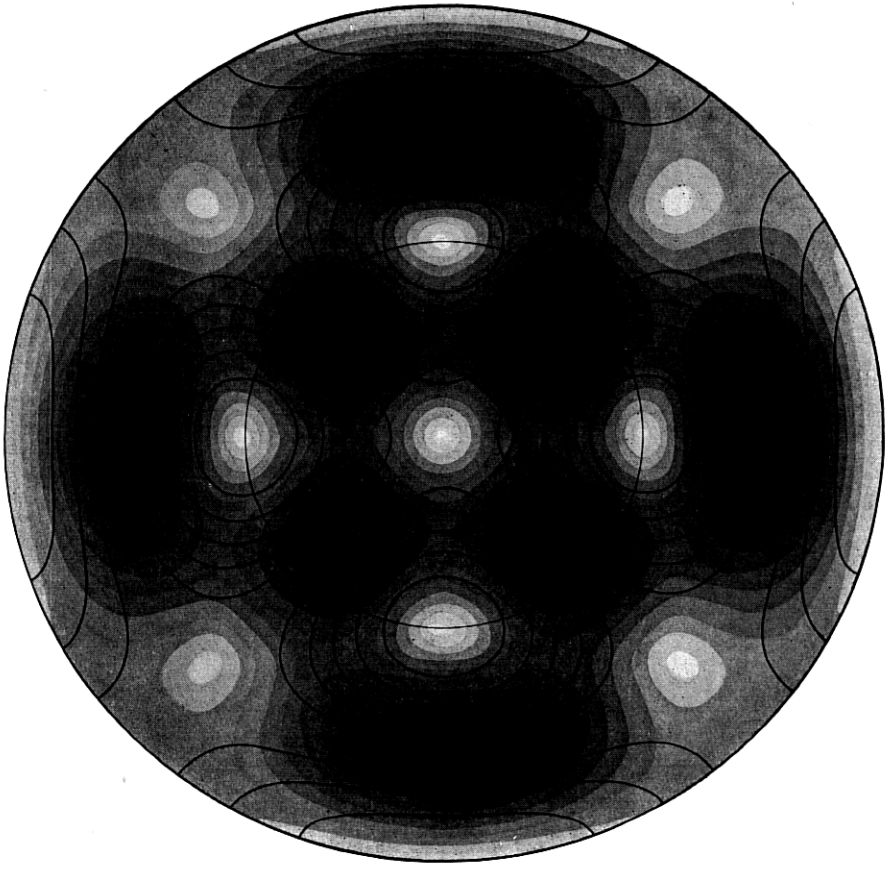

Fig. 44—TE 22 mode.

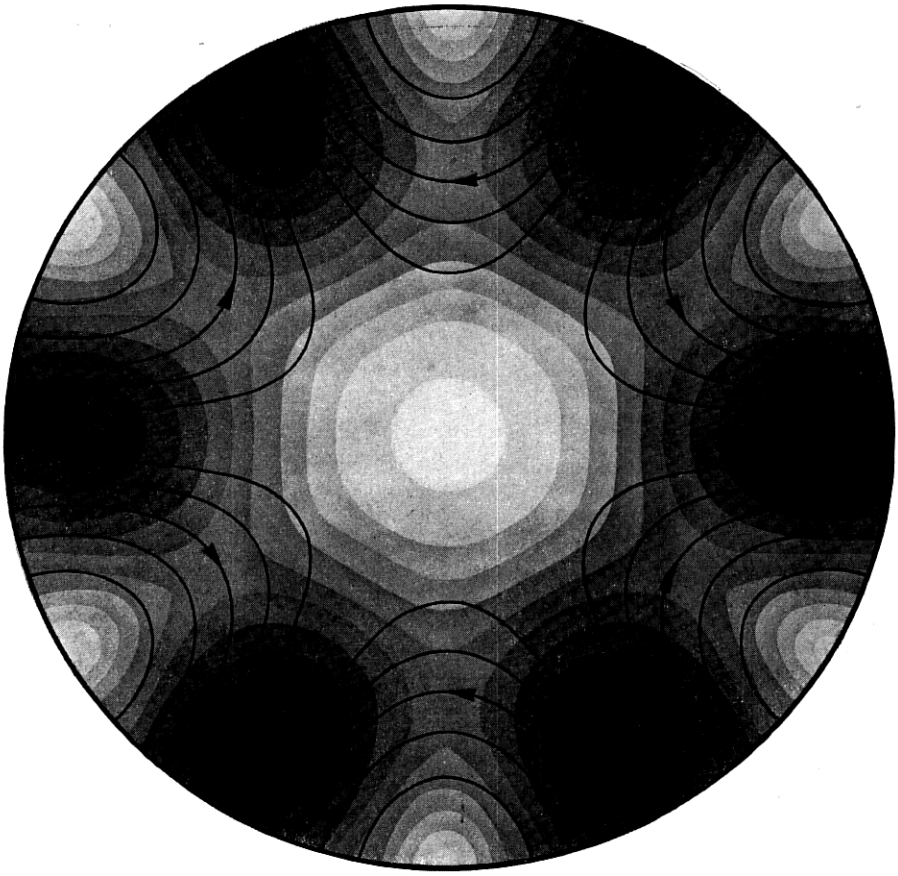

Fig. 45—TE 31 mode.

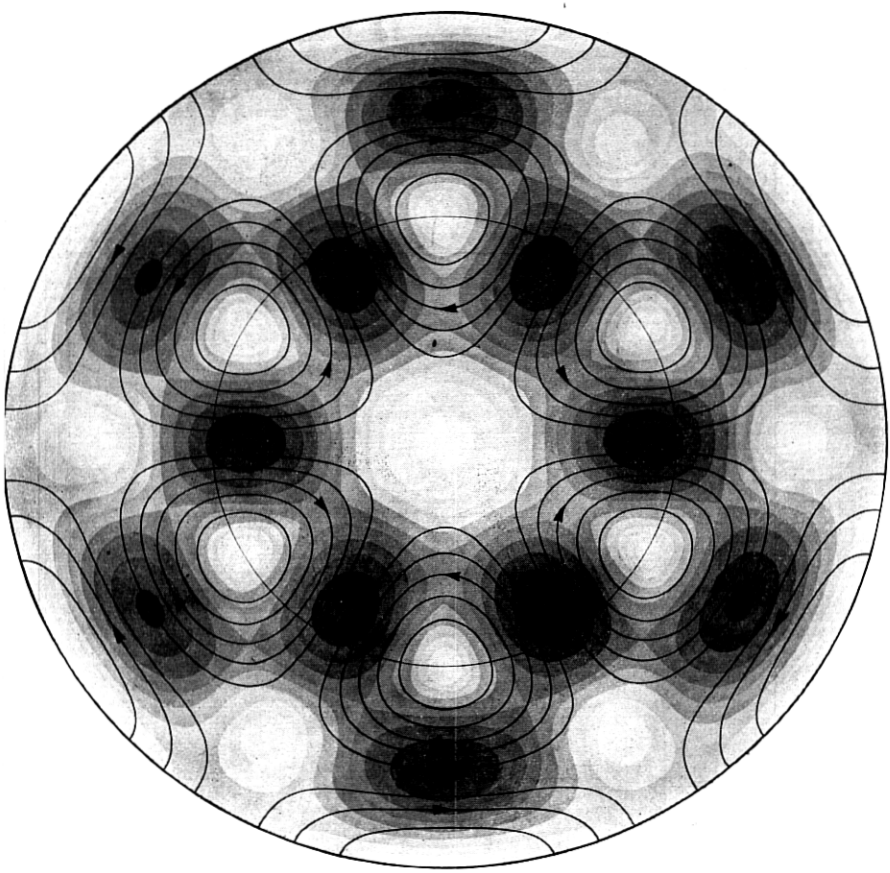

Fig. 46—TE 32 mode.

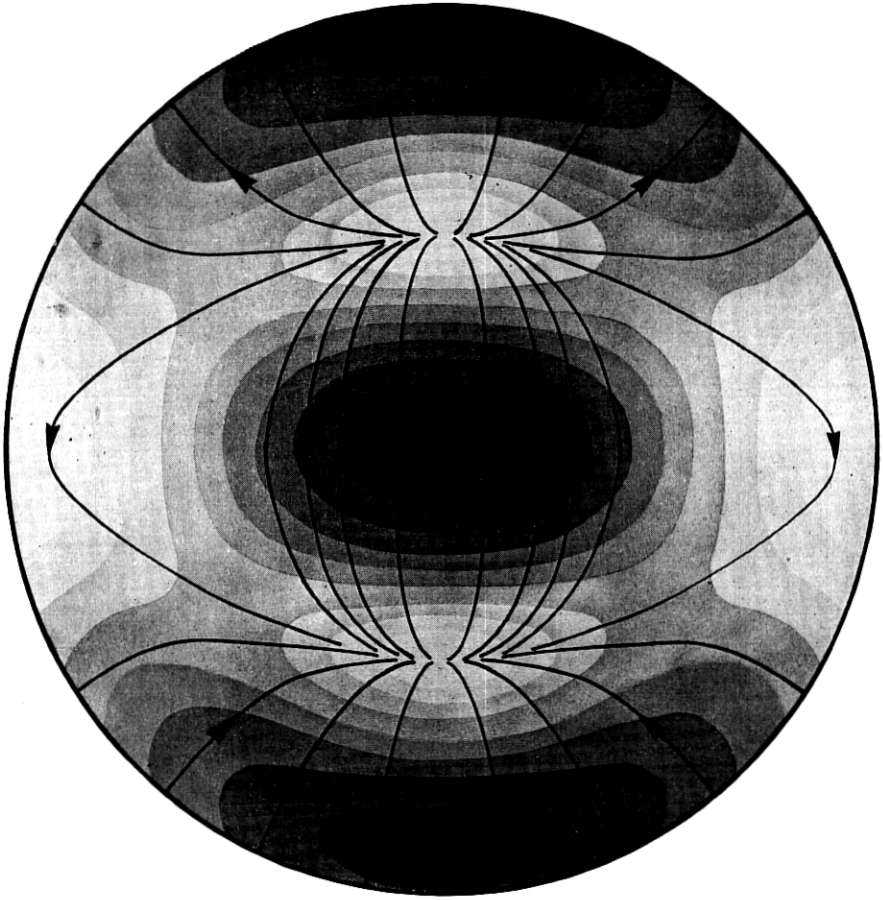

Fig. 47—TM 11 mode.

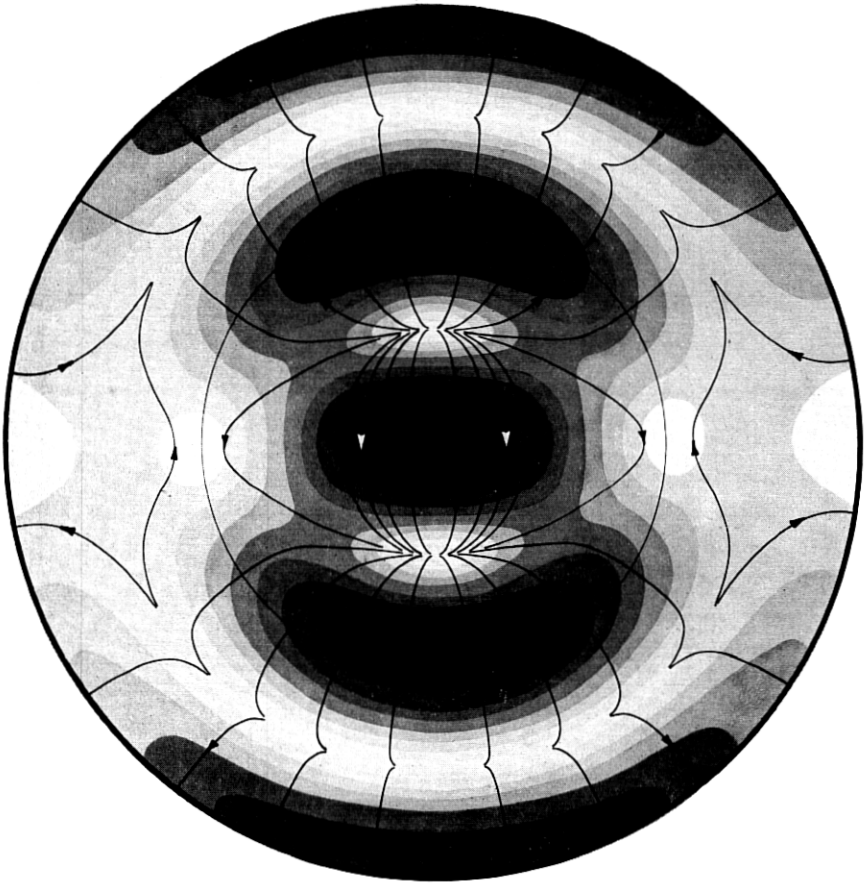

Fig. 48—TM 12 mode.

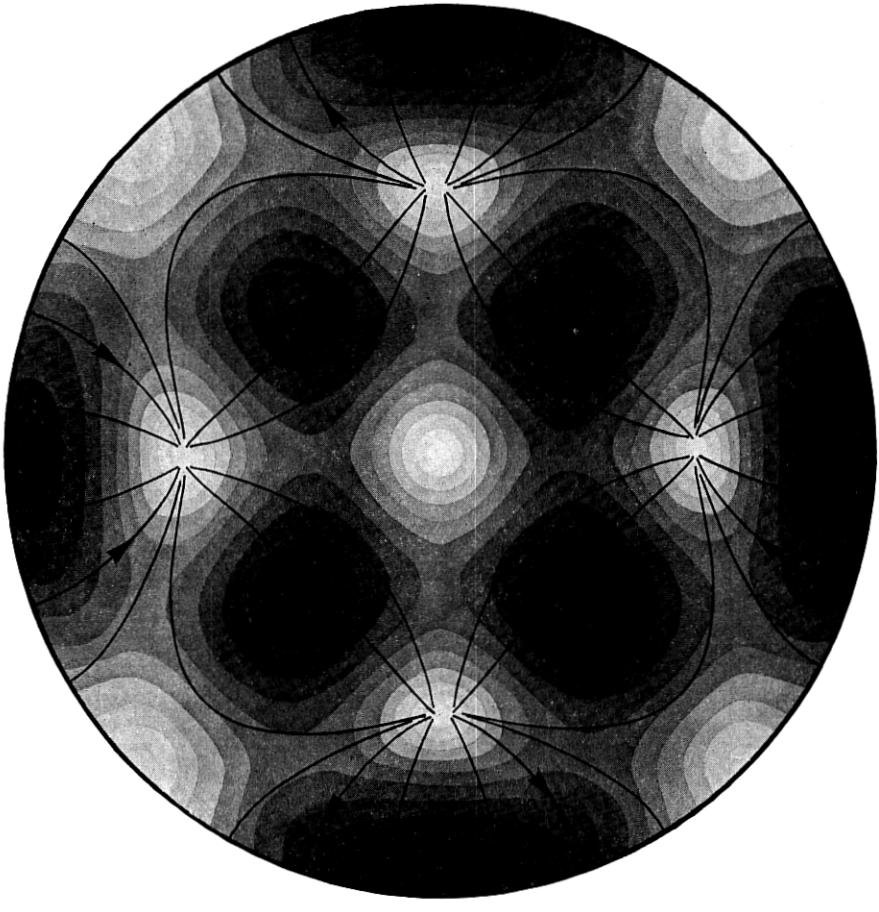

Fig. 49—TM 21 mode

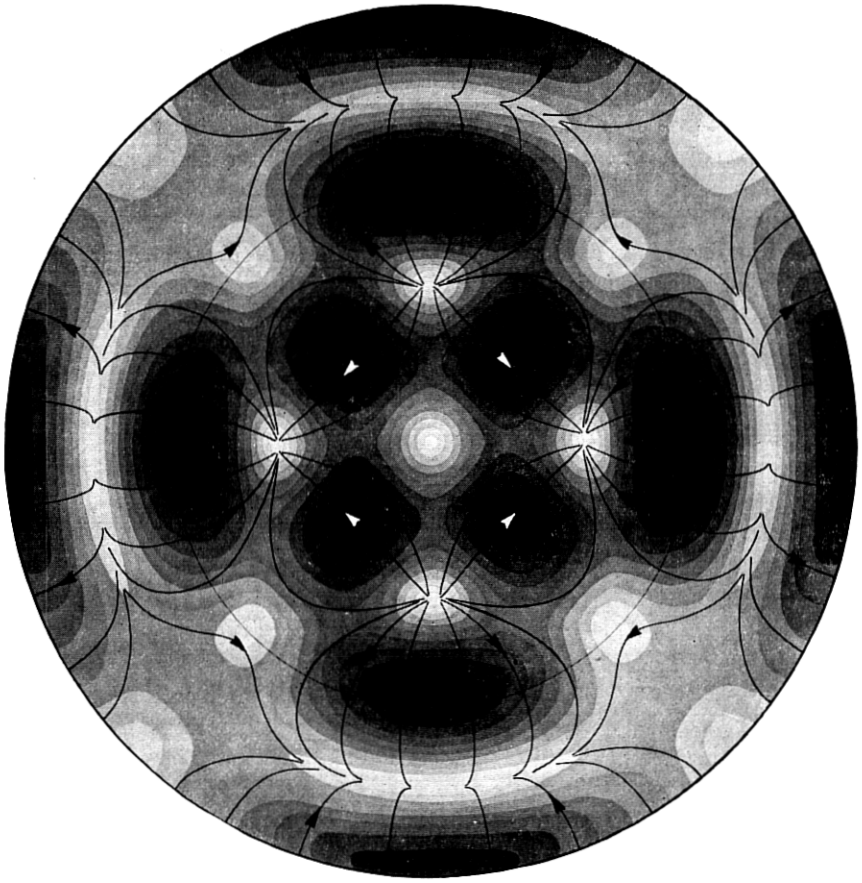

Fig. 50—TM 22 mode.

APPENDIX

INTEGRATION OF $\int_0^x \frac{J_\ell(x)}{J'_\ell(x)}\,dx$

The discussion here is concerned only with integral values of $\ell > 0$. The integral is not simply expressible in terms of known (i.e., tabulated) functions, hence what amounts to a series expansion is used. The method follows Ludinegg[1] who gives the details for $\ell = 1$.

The value of the integrand at $x = 0$ is first discussed. For $\ell = 1$, $J_1(0) = 0$ and $J'_1(0) = 0.5$, hence the integrand has the value zero. For $\ell > 1$, both numerator and denominator are zero, hence the value is indeterminate. Evaluation by $(\ell - 1)$ differentiations of numerator and denominator separately leads to the result that the integrand (and the integral also) is zero at $x = 0$ for all ℓ.

We now introduce a constant $p\ell$ and a function $\phi\ell(x)$ which are such that the following equation is satisfied, at least for a certain range of values of x:

$$J_\ell = -p\ell\left(J''_\ell - \frac{(\ell - 1)J'_\ell}{x}\right) + \phi\ell J'_\ell. \tag{1}$$

Denote the desired integral by $F\ell(x)$, i.e.:

$$F\ell(x) = \int_0^x \frac{J_\ell(x)}{J'_\ell(x)}\,dx. \tag{2}$$

Then substitution of (1) into (2) yields:

$$F_\ell = -p\ell\left[\log \frac{J'_\ell}{x^{(\ell-1)}}\right]_0^x + \int_0^x \phi\ell\,dx. \tag{3}$$

For $x = 0$, $J'_\ell/x^{(\ell-1)}$ is indeterminate, but evaluation by differentiating numerator and denominator separately $(\ell - 1)$ times gives the value $1/2^\ell(\ell - 1)!$

If we can now arrange matters so that $\phi\ell$ remains finite in the range $(0, x)$, its integration can be carried out, a) by expansion into a power series and integration term-by-term, or, b) by numerical integration.

Solving (1) for $\phi\ell$ one obtains

$$\phi\ell = \frac{J_\ell + p\ell\left(J''_\ell - \dfrac{(\ell - 1)J'_\ell}{x}\right)}{J'_\ell}. \tag{4}$$

Equation (4) becomes indeterminate at $x = 0$, when $\ell > 1$. Evaluation by differentiating numerator and denominator separately ℓ times shows $\phi\ell(0) = 0$.

[1] *Hochfrequenztech. u. Elektroak.*, V. 62, pp. 38–44, Aug. 1943.

At the first zero of J_ℓ' (the value of x at a zero of J_ℓ' will be denoted by r), ϕ_ℓ is held finite by choice of the value of p_ℓ. It is clear that (4) becomes indeterminate at $x = r$, if

$$p_\ell = -\frac{J_\ell(r)}{J_\ell''(r)}. \tag{5}$$

Since J_ℓ satisfies the differential equation

$$J_\ell'' + \frac{1}{x} J_\ell' + (1 - \ell^2/x^2) J_\ell = 0 \tag{6}$$

and $J_\ell'(r) = 0$, one has by substitution

$$p_\ell = \frac{r^2}{r^2 - \ell^2}. \tag{7}$$

Values of p for several cases are:

ℓ	=	1	2	3	4	1		1
r_1	=	1.841	3.054	4.201	5.318	r_2 = 5.331	r_3 =	8.536
p_ℓ	=	1.418	1.751	2.040	2.303	1.036		1.014
$\phi_\ell(r)$	=	−0.126	−0.286	−0.446	−0.604	−0.180		−0.115

Evaluation of $\phi_\ell(r)$ by the usual process[2] gives:

$$\phi_\ell(r) = \frac{-r\ell(r^2 - \ell^2 - 2\ell)}{(r^2 - \ell^2)^2} \tag{8}$$

Values of $\phi_\ell(r)$ are given in the preceding table.

Since ϕ_ℓ is finite at the origin and at the first zero of J_ℓ', it may be expanded into a Maclaurin series whose radius of convergence does not, however, exceed the value of x at the second zero of J_ℓ'. Alternatively, by choosing p_ℓ to keep ϕ_ℓ finite at the second (or k^{th}) zero of J_ℓ' it may be expanded into a Taylor series about some point in the interval between the first (or $(k-1)^{th}$) and third (or $(k+1)^{th}$) zeros. Expansions about the origin are given in Table I.

Unfortunately, the convergence of these power series is so slow that they are not very useful. Instead, equation (4) is used to calculate ϕ_ℓ and $\int \phi_\ell \, dx$ is obtained by numerical integration.

With p_ℓ fixed to hold ϕ_ℓ finite at the first root, r_1, of J_ℓ', it is soon found that ϕ_ℓ becomes infinite at the higher roots. This is because different values

[2] Substitute (6) into (4) to eliminate J_ℓ''; differentiate numerator and denominator separately; use (6) to eliminate J_ℓ; allow $x \to r$, using $J_\ell'(r) = 0$ and value of p_ℓ from (7).

of p are required at the different roots, as shown for $\ell = 1$ in the table above. A logical extension would therefore be to make p a function of x such that it takes on the required values at $r_1, r_2, r_3, \cdots$. When this is done and $p_\ell(x)$ is introduced into (1) and (2), one has to integrate

$$\int \frac{p(x)J''(x)}{J'(x)}\,dx$$

and this is intractable.[3]

Hence $p(x)$ is made a discontinuous function, such that p has the value p_1 corresponding to r_1 for values of x from zero to a point b_1 between r_1 and r_2; the value p_2 corresponding to r_2 for values of x from b_1 to a point b_2 between r_2 and r_3; and so forth. This introduces discontinuities in ϕ. No discontinuities exist, however, in the function

$$G_\ell = e^{-F}\ell \tag{9}$$

which is given in Table II. The calculations were made by Miss F. C. Larkey; numerical integration was according to Weddle's rule.

Within the limits of this tabulation, then, G_ℓ and F_ℓ are now considered to be known functions.

TABLE I

POWER SERIES EXPANSIONS OF $\phi_\ell(x)$

$$\phi_1(x) = \left(1 - \frac{3p}{4}\right)x + \left(\frac{1}{4} - \frac{17p}{96}\right)x^3 + \left(\frac{7}{96} - \frac{79p}{1536}\right)x^5 + \cdots$$

$$= -0.063813x - 0.001178x^3 - 0.0000358x^5 - \cdots$$

$$\phi_2(x) = \left(\frac{1}{2} - \frac{p}{3}\right)x + \left(\frac{1}{24} - \frac{7p}{288}\right)x^3 + \left(\frac{5}{1152} - \frac{169p}{17280}\right)x^5 + \cdots$$

$$= +0.15451x + 0.01648x^3 - 0.00580x^5 - \cdots$$

$$\phi_3(x) = \left(\frac{1}{3} - \frac{5p}{24}\right)x + \left(\frac{1}{72} - \frac{41p}{5760}\right)x^3 + \left(\frac{13}{17280} - \frac{103p}{276480}\right)x^5 + \cdots$$

$$= +0.12210x + 0.00667x^3 + 0.00375x^5 - \cdots .$$

[3] Unless $p = b + cJ'$ (b and c constants), which is not of any use.

TABLE II

VALUES OF $F_1(x) = \int_0^x \frac{J_1(x)}{J_1'(x)}\,dx$; $G_1(x) = e^{-F_1}$

$F_1(x)$

x	0	.1	.2	.3	.4	.5	.6	.7	.8	.9
0	• 0	0050	0201	0455	0816	1291	1887	2616	3493	4539
1	5782	7261	9036	1.1192	1.3874	1.7336	2.2103	2.9577	4.6961	4.1846
2	2.7727	2.0801	1.6199	1.2775	1.0073	7864	6018	4454	3117	1970
3	0987	0147	−0564	−1157	−1640	−2018	−2296	−2475	−2556	−2537
4	−2416	−2188	−1845	−1377	−0769	0	+0960	2153	3646	5549
5	8060	1.1595	1.7307	3.2014	2.3851	1.4478	9635	6373	3939	2024
6	0470	−0812	−1879	−2768	−3506	−4111	−4594	−4966	−5233	−5398
7	−5463	−5429	−5292	−5049	−4693	−4214	−3598	−2826	−1868	−0685
8	+0789	2657	5107	8530	1.3992	2.7313	2.1565	1.1974	7154	3942
9	1562	−0300	−1802	−3034	−4053	−4897	−5590	−6150	−6591	−6921

$G_1(x)$

x	0	.1	.2	.3	.4	.5	.6	.7	.8	.9
0	1.0000	9950	9801	9555	9216	8789	8280	7698	7052	6351
1	5609	4838	4051	3265	2497	1766	1097	0519	0091	0152
2	0625	1249	1979	2787	3652	4555	5478	6406	7322	8212
3	9060	9854	1.0580	1.1226	1.1781	1.2236	1.2581	1.2808	1.2912	1.2888
4	1.2733	1.2445	1.2026	1.1476	1.0799	1.0000	9085	8063	6945	5741
5	4467	3136	1772	0407	0921	2351	3816	5287	6744	8168
6	9541	1.0846	1.2067	1.3190	1.4200	1.5084	1.5831	1.6432	1.6877	1.7157
7	1.7269	1.7209	1.6976	1.6568	1.5989	1.5241	1.4331	1.3265	1.2054	1.0709
8	9241	7667	6001	4261	2468	0613	1157	3020	4890	6742
9	8554	1.0304	1.1974	1.3545	1.4998	1.6318	1.7489	1.8497	1.9330	1.9978

VALUES OF $F_2(x) = \int_0^x \frac{J_2(x)}{J_2'(x)}\,dx$; $G_2(x) = e^{-F_2}$

$F_2(x)$

x	0	.1	.2	.3	.4	.5	.6	.7	.8	.9
0	0	0025	0100	0226	0403	0632	0914	1251	1645	2097
1	2612	3192	3840	4563	5365	6253	7236	8323	9528	1.0866
2	1.2357	1.4008	1.5913	1.8061	2.0541	2.3456	2.6972	3.1380	3.7263	4.6110
3	6.4527	6.7644	4.7528	3.8572	3.2808	2.8597	2.5316	2.2658	2.0451	1.8590
4	1.7002	1.5641	1.4470	1.3466	1.2607	1.1881	1.1275	1.0783	1.0396	1.0112
5	9928	9843	9858	9974	1.0196	1.0530	1.0985	1.1573	1.2311	1.3223
6	1.4345	1.5726	1.7447	1.9640	2.2555	2.6743	3.3910	6.5119	3.5122	2.7144
7	2.2595	1.9432	1.7034	1.5131	1.3579	1.2294	1.1223	1.0328	.9586	.8977
8	.8490	.8115	.7846	.7679	.7612	.7645	.7779	.8020	.8372	.8845
9	.9452	1.0212	1.1149	1.2301	1.3725	1.5512	1.7817	2.0950	2.5660	3.4864

$G_2(x)$

x	0	.1	.2	.3	.4	.5	.6	.7	.8	.9
0	1.0000	9975	9900	9777	9605	9388	9127	8824	8483	8108
1	7701	7267	6811	6336	5848	5351	4850	4350	3856	3373
2	2906	2459	2036	1643	1282	0958	0674	0434	0241	0099
3	0017	0012	0086	0211	0376	0573	0795	1037	1294	1558
4	1826	2093	2353	2601	2834	3048	3238	3402	3536	3638
5	3705	3737	3731	3688	3607	3489	3334	3143	2920	2665
6	2383	2075	1747	1403	1048	0690	0337	0015	0298	0662
7	1044	1432	1821	2202	2572	2925	3255	3560	3834	4075
8	4278	4442	4563	4640	4671	4656	4593	4484	4329	4129
9	3886	3602	3280	2923	2535	2120	1683	1231	0768	0306

VALUES OF $F_3(x) = \int_0^x \frac{J_3(x)}{J_3'(x)}\,dx$; $G_3(x) = e^{-F_3}$

$F_3(x)$

x	0	.1	.2	.3	.4	.5	.6	.7	.8	.9
0	0	0017	0067	0152	0268	0420	0604	0826	1081	1373
1	1703	2070	2476	2922	3410	3942	4518	5141	5814	6539
2	7319	8158	9060	1.0028	1.1070	1.2192	1.3401	1.4706	1.6118	1.7650
3	1.9321	2.1150	2.3165	2.5402	2.7908	3.0752	3.4034	3.7905	4.2624	4.8669
4	5.7117	7.1373	16.2303	7.2383	5.8409	5.0409	4.4852	4.0643	3.7292	3.4543
5	3.2239	3.0282	2.8605	2.7160	2.5913	2.4838	2.3914	2.3128	2.2467	2.1922
6	2.1487	2.1156	2.0927	2.0798	2.0768	2.0838	2.1012	2.1293	2.1685	2.2208
7	2.2864	2.3674	2.4664	2.5868	2.7340	2.9159	3.1460	3.4491	3.8790	4.5950
8	6.9408	4.9414	4.0348	3.5348	3.1912	2.9324	2.7276	2.5608	2.4227	2.3074
9	2.2108	2.1302	2.0637	2.0097	1.9676	1.9361	1.9147	1.9036	1.9025	1.9115

$G_3(x)$

x	0	.1	.2	.3	.4	.5	.6	.7	.8	.9
0	1.0000	9983	9933	9849	9734	9589	9413	9208	8975	8717
1	8434	8130	7806	7466	7110	6742	6365	5980	5591	5200
2	4810	4423	4041	3668	3305	2955	2618	2298	1995	1712
3	1448	1206	0986	0789	0614	0462	0333	0226	0141	0077
4	0033	0008	0000	0007	0029	0065	0113	0172	0240	0316
5	0398	0484	0572	0661	0749	0834	0915	0990	1057	1117
6	1166	1206	1233	1250	1253	1244	1223	1189	1143	1085
7	1016	0937	0849	0753	0650	0542	0430	0318	0207	0101
8	0010	0071	0177	0292	0411	0533	0654	0772	0887	0995
9	1096	1188	1270	1340	1398	1443	1474	1490	1492	1479

Table III

Bessel Functions of The First Kind

$J_0(x)$

x	.0	.1	.2	.3	.4	.5	.6	.7	.8	.9
0	+1.0	9975	9900	9776	9604	+9385	9120	8812	8463	8075
1	+7652	7196	6711	6201	5669	+5118	4554	3980	3400	2818
2	+2239	1666	1104	0555	0025	−0484	0968	1424	1850	2243
3	−2601	2921	3202	3443	3643	−3801	3918	3992	4026	4018
4	−3971	3887	3766	3610	3423	−3205	2961	2693	2404	2097
5	−1776	1443	1103	0758	0412	−0068	+0270	+0599	+0917	+1220
6	+1506	1773	2017	2238	2433	+2601	2740	2851	2931	2981
7	+3001	2991	2951	2882	2786	+2663	2516	2346	2154	1944
8	+1717	1475	1222	0960	0692	+0419	0146	−0125	−0392	−0653
9	−0903	1142	1367	1577	1768	−1939	2090	2218	2323	2403

$J_1(x)$

x	.0	.1	.2	.3	.4	.5	.6	.7	.8	.9
0	+0	0499	0995	1483	1960	+2423	2867	3290	3688	4059
1	+4401	4709	4983	5220	5419	+5579	5699	5778	5815	5812
2	+5767	5683	5560	5399	5202	+4971	4708	4416	4097	3754
3	+3391	3009	2613	2207	1792	+1374	0955	0538	0128	−0272
4	−0660	1033	1386	1719	2028	−2311	2566	2791	2985	3147
5	−3276	3371	3432	3460	3453	−3414	3343	3241	3110	2951
6	−2767	2559	2329	2081	1816	−1538	1250	0953	0652	0349
7	−0047	+0252	+0543	+0826	+1096	+1352	1592	1813	2014	2192
8	+2346	2476	2580	2657	2708	+2731	2728	2697	2641	2559
9	+2453	2324	2174	2004	1816	+1613	1395	1166	0928	0684

$J_2(x)$

x	.0	.1	.2	.3	.4	.5	.6	.7	.8	.9
0	+0	0012	0050	0112	0197	0306	0437	0588	0758	0946
1	+1149	1366	1593	1830	2074	2321	2570	2817	3061	3299
2	+3528	3746	3951	4139	4310	4461	4590	4696	4777	4832
3	+4861	4862	4835	4780	4697	4586	4448	4283	4093	3879
4	+3641	3383	3105	2811	2501	2178	1846	1506	1161	0813
5	+0466	0121	−0217	−0547	−0867	−1173	1464	1737	1990	2221
6	−2429	2612	2769	2899	3001	3074	3119	3135	3123	3082
7	−3014	2920	2800	2656	2490	2303	2097	1875	1638	1389
8	−1130	0864	0593	0320	0047	+0223	0488	0745	0993	1228
9	+1448	1653	1840	2008	2154	2279	2380	2458	2512	2542

$J_3(x)$

x	.0	.1	.2	.3	.4	.5	.6	.7	.8	.9
0	+0	0	0002	0006	0013	0026	0044	0069	0102	0144
1	+0196	0257	0329	0411	0505	0610	0725	0851	0988	1134
2	+1289	1453	1623	1800	1981	2166	2353	2540	2727	2911
3	+3091	3264	3431	3588	3734	3868	3988	4092	4180	4250
4	+4302	4333	4344	4333	4301	4247	4171	4072	3952	3811
5	+3648	3466	3265	3046	2811	2561	2298	2023	1738	1446
6	+1148	0846	0543	0240	−0059	−0353	0641	0918	1185	1438
7	−1676	1896	2099	2281	2442	2581	2696	2787	2853	2895
8	−2911	2903	2869	2811	2730	2626	2501	2355	2190	2007
9	−1809	1598	1374	1141	0900	0653	0403	0153	+0097	+0343

$J_4(x)$

x	.0	.1	.2	.3	.4	.5	.6	.7	.8	.9
0	+0	0	0	0	0001	0002	0003	0006	0010	0016
1	+0025	0036	0050	0068	0091	0118	0150	0188	0232	0283
2	+0340	0405	0476	0556	0643	0738	0840	0950	1067	1190
3	+1320	1456	1597	1743	1892	2044	2198	2353	2507	2661
4	+2811	2958	3100	3236	3365	3484	3594	3693	3780	3853
5	+3912	3956	3985	3996	3991	3967	3926	3866	3788	3691
6	+3576	3444	3294	3128	2945	2748	2537	2313	2077	1832
7	+1578	1317	1051	0781	0510	0238	−0031	−0297	−0557	−0810
8	−1054	1286	1507	1713	1903	2077	2233	2369	2485	2581
9	−2655	2707	2736	2743	2728	2691	2633	2553	2453	2334

$J_5(x)$

x	.0	.1	.2	.3	.4	.5	.6	.7	.8	.9
0	+0	0	0	0	0	0	0	0	0001	0001
1	+0002	0004	0006	0009	0013	0018	0025	0033	0043	0055
2	+0070	0088	0109	0134	0162	0195	0232	0274	0321	0373
3	+0430	0493	0562	0637	0718	0804	0897	0995	1098	1207
4	+1321	1439	1561	1687	1816	1947	2080	2214	2347	2480
5	+2611	2740	2865	2986	3101	3209	3310	3403	3486	3559
6	+3621	3671	3708	3731	3741	3736	3716	3680	3629	3562
7	+3479	3380	3266	3137	2993	2835	2663	2478	2282	2075
8	+1858	1632	1399	1161	0918	0671	0424	0176	−0070	−0313
9	−0550	0782	1005	1219	1422	1613	1790	1953	2099	2229

$J_6(x)$

x	.0	.1	.2	.3	.4	.5	.6	.7	.8	.9
0	0	0	0	0	0	0	0	0	0	0
1	0	0	0001	0001	0002	0002	0003	0005	0007	0009
2	0012	0016	0021	0027	0034	0042	0052	0065	0079	0095
3	0114	0136	0160	0188	0219	0254	0293	0336	0383	0435
4	0491	0552	0617	0688	0763	0843	0927	1017	1111	1209
5	1310	1416	1525	1637	1751	1868	1986	2104	2223	2341
6	2458	2574	2686	2795	2900	2999	3093	3180	3259	3330
7	3392	3444	3486	3516	3535	3541	3535	3516	3483	3436
8	3376	3301	3213	3111	2996	2867	2725	2571	2406	2230
9	2043	1847	1644	1432	1215	0993	0768	0540	0311	0082

$J_7(x)$

x	.0	.1	.2	.3	.4	.5	.6	.7	.8	.9
0	0	0	0	0	0	0	0	0	0	0
1	0	0	0	0	0	0	0	0001	0001	0001
2	0002	0002	0003	0004	0006	0008	0010	0013	0016	0020
3	0025	0031	0038	0047	0056	0067	0080	0095	0112	0130
4	0152	0176	0202	0232	0264	0300	0340	0382	0429	0479
5	0534	0592	0654	0721	0791	0866	0945	1027	1113	1203
6	1296	1392	1491	1592	1696	1801	1908	2015	2122	2230
7	2336	2441	2543	2643	2739	2832	2919	3001	3076	3145
8	3206	3259	3303	3337	3362	3376	3379	3371	3351	3319
9	3275	3218	3149	3068	2974	2868	2750	2620	2480	2328

$J_1'(x)$

x	.0	.1	.2	.3	.4	.5	.6	.7	.8	.9
0	+5000	4981	4925	4832	4703	4539	4342	4112	3852	3565
1	+3251	2915	2559	2185	1798	1399	0992	0581	0169	−0241
2	−0645	1040	1423	1792	2142	2472	2779	3060	3314	3538
3	−3731	3891	4019	4112	4170	4194	4183	4138	4059	3948
4	−3806	3635	3435	3210	2962	2692	2404	2100	1782	1455
5	−1121	0782	0443	0105	+0227	+0552	0867	1168	1453	1721
6	+1968	2192	2393	2568	2717	2838	2930	2993	3027	3032
7	+3007	2955	2875	2769	2638	2483	2307	2110	1896	1666
8	+1423	1169	0908	0640	0369	0098	−0171	−0435	−0692	−0940
9	−1176	1398	1604	1792	1961	2109	2235	2338	2417	2472

$J_2'(x)$

x	.0	.1	.2	.3	.4	.5	.6	.7	.8	.9
0	+0	0250	0497	0739	0974	1199	1412	1610	1793	1958
1	+2102	2226	2327	2404	2457	2485	2487	2463	2414	2339
2	+2239	2115	1968	1799	1610	1402	1178	0938	0685	0422
3	+0150	−0128	−0409	−0691	−0971	−1247	1516	1777	2026	2261
4	−2481	2683	2865	3026	3165	3279	3368	3432	3469	3479
5	−3462	3419	3349	3253	3132	2988	2821	2632	2424	2199
6	−1957	1702	1436	1161	0879	0592	0305	0018	+0266	+0544
7	+0814	1074	1321	1553	1769	1967	2144	2300	2434	2543
8	+2629	2689	2725	2734	2719	2679	2614	2526	2415	2283
9	+2131	1961	1774	1572	1358	1133	0899	0659	0416	0170

$J_3'(x)$

x	.0	.1	.2	.3	.4	.5	.6	.7	.8	.9
0	+0	0006	0025	0056	0098	0152	0217	0291	0374	0465
1	+0562	0665	0772	0881	0991	1102	1210	1315	1415	1508
2	+1594	1671	1737	1792	1833	1861	1875	1873	1855	1821
3	+1770	1703	1619	1519	1403	1271	1125	0965	0793	0609
4	+0415	0212	0003	−0213	−0432	−0653	0874	1094	1310	1520
5	−1723	1918	2101	2272	2429	2570	2695	2801	2889	2956
6	−3003	3028	3031	3013	2973	2911	2828	2724	2600	2457
7	−2296	2118	1925	1719	1500	1270	1033	0789	0540	0289
8	−0038	+0211	+0457	+0696	+0928	+1150	1360	1557	1739	1904
9	+2052	2180	2288	2376	2441	2485	2507	2506	2483	2438

$J_4'(x)$

x	.0	.1	.2	.3	.4	.5	.6	.7	.8	.9
0	+0	0	0001	0003	0007	0013	0022	0034	0051	0071
1	+0097	0126	0161	0201	0246	0296	0350	0409	0473	0539
2	+0610	0682	0757	0833	0909	0985	1060	1133	1203	1269
3	+1330	1385	1434	1475	1508	1532	1545	1549	1541	1522
4	+1490	1447	1391	1323	1243	1150	1045	0929	0802	0665
5	+0518	0363	0200	0030	−0145	−0324	0506	0690	0874	1057
6	−1237	1412	1582	1745	1900	2045	2178	2299	2407	2500
7	−2577	2638	2683	2709	2718	2708	2679	2633	2568	2485
8	−2385	2267	2134	1986	1824	1649	1462	1265	1060	0847
9	−0629	0408	0184	+0039	+0261	+0480	0694	0900	1098	1286

$J_5'(x)$

x	.0	.1	.2	.3	.4	.5	.6	.7	.8	.9
0	+0	0	0	0	0	0001	0002	0003	0005	0008
1	+0012	0018	0025	0034	0045	0058	0073	0092	0113	0137
2	+0164	0194	0228	0265	0305	0348	0394	0443	0494	0548
3	+0603	0660	0718	0777	0836	0895	0952	1008	1062	1113
4	+1160	1203	1242	1274	1301	1321	1333	1338	1335	1322
5	+1301	1270	1230	1180	1120	1050	0970	0881	0782	0675
6	+0559	0435	0304	0166	0023	−0126	0278	0433	0591	0749
7	−0907	1064	1217	1368	1513	1652	1783	1906	2020	2123
8	−2215	2294	2360	2412	2449	2472	2479	2470	2446	2405
9	−2349	2277	2190	2088	1972	1842	1700	1546	1382	1208

$J_6'(x)$

x	.0	.1	.2	.3	.4	.5	.6	.7	.8	.9
0	+0	0	0	0	0	0	0	0	0	0001
1	+0001	0002	0003	0004	0006	0009	0012	0016	0021	0027
2	+0034	0043	0053	0065	0078	0094	0111	0130	0152	0176
3	+0202	0231	0262	0295	0331	0368	0408	0450	0493	0538
4	+0585	0632	0680	0728	0776	0823	0870	0916	0959	1000
5	+1039	1074	1105	1132	1155	1172	1183	1188	1187	1178
6	+1163	1139	1108	1069	1022	0967	0904	0833	0753	0666
7	+0572	0470	0362	0247	0127	0002	−0128	−0261	−0397	−0535
8	−0674	0813	0952	1088	1222	1352	1478	1597	1710	1816
9	−1912	2000	2077	2143	2198	2240	2270	2287	2290	2279

TABLE IV

RELATIVE RADIUS FOR MAXIMUM OF ρI_p^2

Mode			
TE 11	.737		
12	.982	.254	
13	.993	.613	.159
21	.894		
22	.988	.407	
23	.995	.664	.274
31	.937		
32	.991	.491	
41	.956		
42	.993	.548	
51	.967		
61	.974		
TM 01	.901		
02	.983	.393	
03	.993	.627	.250
11	.961		
12	.989	.525	
13	.995	.682	.362
21	.977		
22	.992	.596	
31	.984		
32	.994	.643	
41	.988		
51	.990		
61	.992		